

Binary-binary scattering in the secular limit

Adrian S. Hamers¹^{*} and Johan Samsing²[†]

¹Max-Planck-Institut für Astrophysik, Karl-Schwarzschild-Str. 1, 85741 Garching, Germany

²Niels Bohr International Academy, The Niels Bohr Institute, Blegdamsvej 17, DK-2100, Copenhagen, Denmark

Accepted 2020 March 9. Received 2020 March 6; in original form 2020 February 12

ABSTRACT

Binary-binary interactions are important in a number of astrophysical contexts including dense stellar systems such as globular clusters. Although less frequent than binary-single encounters, binary-binary interactions lead to a much richer range of possibilities such as the formation of stable triple systems. Here, we focus on the regime of distant binary-binary encounters, i.e., two binaries approaching each other on an unbound orbit with a periastris distance Q much larger than the internal binary separations. This ‘secular’ regime gives rise to changes in the orbital eccentricities and orientations, which we study using analytic considerations and numerical integrations. We show that ‘direct’ interactions between the three orbits only occur starting at a high expansion order of the Hamiltonian (hexadecupole order), and that the backreaction of the outer orbit on the inner two orbits at lower expansion orders is weak. Therefore, to good approximation, one can obtain the changes of each orbit by using previously-known analytic results for binary-single interactions, and replacing the mass of the third body with the total mass of the companion binary. Nevertheless, we find some dependence of the ‘binarity’ of the companion binary, and derive explicit analytic expressions for the secular changes that are consistent with numerical integrations. In particular, the eccentricity and inclination changes of orbit 1 due to orbit 2 scale as $\epsilon_{\text{SA},1}(a_2/Q)^2[m_3m_4/(m_3+m_4)^2]$, where $\epsilon_{\text{SA},1}$ is the approximate quadrupole-order change, and a_2 and (m_3, m_4) are the companion binary orbital semimajor axis and component masses, respectively. Our results are implemented in several PYTHON scripts that are freely available.

Key words: gravitation – celestial mechanics – stars: kinematics and dynamics – globular clusters: general – stars: black holes

1 INTRODUCTION

Dense stellar systems such as open and globular clusters are host to a wide range of dynamical interactions involving bound objects such as binaries-single scattering, as well as scattering involving higher-order systems, e.g., binary-binary scattering. Since such interactions are believed to lead to mergers of black holes (BHs) and neutron stars (NSs) (e.g., Sigurdsson & Hernquist 1993; Portegies Zwart & McMillan 2000; O’Leary et al. 2006; Ziosi et al. 2014; Rodriguez et al. 2015, 2016; Kimpson et al. 2016; Mapelli 2016; Samsing & Ramirez-Ruiz 2017; Samsing et al. 2018b,c; Samsing 2018; Rodriguez et al. 2018; Samsing et al. 2019, interest in them has recently surged with the direct detection of gravitational waves (GWs) from merging black holes (BHs) and neutron stars (NSs; e.g., Abbott et al. 2016b,a, 2017a,d,b,c).

The topic of binary-single scattering has received a great deal of attention in the past decades (e.g., Hut & Bahcall 1983; Hut 1983; Heggie & Hut 1993; Hut 1993; Goodman & Hut 1993; Sigurdsson & Phinney 1993; Davies et al. 1993; McMillan & Hut 1996; Heggie et al. 1996; Kocsis & Levin 2012; Samsing et al. 2018a). Binary-binary encounters have been studied as well, although perhaps with less intensity given its greater complexity. Nevertheless, in star clusters with binary fractions $\gtrsim 10\%$, binary-binary interactions dominate over binary-single interactions (Sigurdsson & Phinney 1993; Leigh & Sills 2011). Furthermore, even if the overall binary fraction of a stellar cluster is low, the binary fraction in the core can be much higher (Leonard 1989; Hut et al. 1992; McMillan & Hut 1994). Binary-binary scattering can also occur in other astrophysical contexts, such as binaries passing by planetary systems in the field (e.g., Li & Adams 2015).

Studies of binary-binary scattering to date (e.g., Mikkola 1983; Hoffer 1983; Mikkola 1984a,b; Alexander 1986; Leonard 1989; Rasio et al. 1995; Bacon et al. 1996; Leigh & Geller 2012, 2015; Antognini & Thompson 2016; Leigh et al. 2017; Ryu et al. 2017; Leigh et al. 2018; Zevin et al. 2019) have mostly focussed on numerical investigations of “strong” scattering, i.e., when the two binaries approach each other sufficiently closely that at least their binding energies change appreciably, and, more generally, leading to complex interactions such as the breakup of binaries, exchange interactions, and the formation of (stable or unstable) triples.

^{*} E-mail: hamers@mpa-garching.mpg.de

[†] E-mail: jsamsing@gmail.com

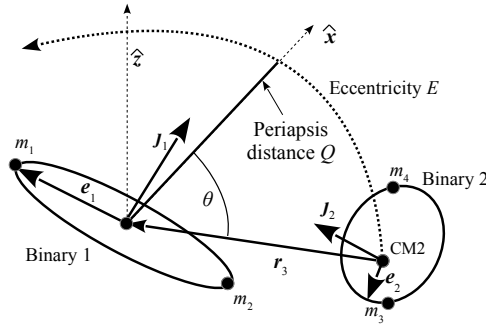


Figure 1. Sketch of the configuration. Two bound binaries (labeled ‘1’ and ‘2’) approach each other on a parabolic or hyperbolic orbit with eccentricity $E \geq 1$ and periapsis distance $Q > a_i$ ($i \in \{1, 2\}$).

However, more distant encounters are more common than the close encounters that give rise to “strong” interactions. In these more distant encounters with periapsis distances $Q \gg a_i$, where a_i ($i \in \{1, 2\}$) are the semimajor axes of the two bound binaries, energy changes are exponentially suppressed (Heggie 1975), whereas angular-momentum changes can still occur. These more distant encounters can be characterised as ‘secular’, i.e., the orbital motion of the components in the bound systems is much faster than the orbital motion of the wider, unbound orbit. These secular encounters have been studied by a number of authors in the context of binary-single encounters (e.g., Heggie & Rasio 1996; Spurzem et al. 2009; Hamers 2018; Geller et al. 2019; Hamers & Samsing 2019a,b). Secular binary-single encounters can have important implications for the properties of binary BH mergers in globular clusters (Samsing et al. 2019). However, to our knowledge, secular effects in binary-binary encounters have not been addressed before.

In this paper, we consider the dynamical evolution of two binaries approaching each other on a parabolic or hyperbolic orbit with a periapsis distance larger than the binaries’ internal separations. In Section 2, we derive expressions for the secular changes in the two binaries based on the expanded and partially-averaged Hamiltonian of the system. In Section 3, we carry out numerical simulations (direct-integration four-body simulations, as well as semianalytic integrations based on the partially-averaged Hamiltonian) and use these to test our analytic expressions. We discuss our results in Section 4, and conclude in Section 5.

2 ANALYTIC CONSIDERATIONS

2.1 Setup

We consider two bound binary systems (their orbits indicated with ‘1’ and ‘2’) that approach each other on an unbound orbit (the latter is referred to as orbit ‘3’, or the ‘outer’ orbit). See Fig. 1 for a sketch. Let the masses of the components in orbit 1 be m_1 and m_2 , respectively, and m_3 and m_4 for orbit 2. For convenience, we introduce the quantities $M_1 \equiv m_1 + m_2$, $M_2 \equiv m_3 + m_4$, and $M_3 \equiv M \equiv M_1 + M_2$. The (initial) semimajor axes and eccentricities of all orbits are denoted with a_i and e_i , where it should be noted that $a_3 < 0$, and $e_3 \geq 1$. Also, to further distinguish between the bound and unbound orbits, we introduce the notation $E \equiv e_3 \geq 1$ for the (initial) outer orbit eccentricity, and $Q \equiv a_3(1 - e_3) > 0$ for the outer orbit periapsis distance. Note that in defining Q and E , we neglect the extended nature of the bound orbits (i.e., approximate the latter as point masses). Evidently, since we are dealing with two binaries instead of two point particles, the latter approximation breaks down as $Q \rightarrow 0$.

Let the relative separation between the two bodies in orbit 1 be denoted with \mathbf{r}_1 ; similarly, the relative separation vector between bodies 3 and 4 in orbit 2 is \mathbf{r}_2 . The outer orbit has a separation vector \mathbf{r}_3 between the two centers of mass of orbits 1 and 2. The instantaneous eccentricity or Laplace-Runge-Lenz vector \mathbf{e}_i is given by $\mathbf{e}_i = [1/(GM_i)] \dot{\mathbf{r}}_i \times (\mathbf{r}_i \times \dot{\mathbf{r}}_i) - \hat{\mathbf{r}}_i$, where dots denote derivatives with respect to time, and hats denote unit vectors. For orbits 1 and 2, the normalized angular-momentum vectors are $\mathbf{J}_i = \mathbf{r}_i \times \dot{\mathbf{r}}_i$, with magnitudes $J_i = \sqrt{1 - e_i^2}$.

Without loss of generality, we assume that the outer orbit is initially oriented with its angular-momentum vector along the z -axis, and the periapsis pointing along the x -axis. In this case, and neglecting the backreaction of the outer orbit due to the quadrupole moment of the inner orbits (see Section 2.4.1 below), the outer orbit is described according to

$$\mathbf{r}_3 = \frac{Q(1+E)}{1+E \cos \theta} [\cos \theta \hat{\mathbf{x}} + \sin \theta \hat{\mathbf{y}}]; \quad (1a)$$

$$\dot{\mathbf{r}}_3 = \sqrt{\frac{GM}{Q(1+E)}} [-\sin \theta \hat{\mathbf{x}} + (E + \cos \theta) \hat{\mathbf{y}}]. \quad (1b)$$

The outer orbit true anomaly θ is related to the physical time t according to

$$dt = \frac{1}{n_3} (E^2 - 1) \frac{1}{(1 + E \cos \theta)^2} d\theta, \quad (2)$$

where $n_3 \equiv \sqrt{GM/|a_3|^3}$ is the hyperbolic mean motion, and $|a_3| = Q/(E - 1)$. The true anomaly θ ranges between $-L$ and L corresponding

to $-\infty < t < \infty$, where

$$L \equiv \arccos\left(-\frac{1}{E}\right). \quad (3)$$

2.2 Hamiltonian

2.2.1 Expansion

In the limit that the two binaries approach each other with a periapsis distance $Q \gg r_1, r_2$, it is appropriate to expand the Hamiltonian of the four-body system in terms of the small ratios $r_1/r_3 \ll 1$, and $r_2/r_3 \ll 1$. The resulting ‘binary-binary’ Hamiltonian is (Hamers et al. 2015, see also Hamers & Portegies Zwart 2016)

$$\begin{aligned} H_{\text{bb}} = & H_{\text{kep}}(m_1, m_2, \mathbf{r}_1, \dot{\mathbf{r}}_1) + H_{\text{kep}}(m_3, m_4, \mathbf{r}_2, \dot{\mathbf{r}}_2) + H_{\text{kep}}(m_1 + m_2, m_3 + m_4, \mathbf{r}_3, \dot{\mathbf{r}}_3) \\ & + H_{\text{quad}}(m_1, m_2, m_3 + m_4, \mathbf{r}_1, \mathbf{r}_3) + H_{\text{quad}}(m_3, m_4, m_1 + m_2, \mathbf{r}_2, \mathbf{r}_3) \\ & + H_{\text{oct}}(m_1, m_2, m_3 + m_4, \mathbf{r}_1, \mathbf{r}_3) + H_{\text{oct}}(m_4, m_3, m_1 + m_2, \mathbf{r}_2, \mathbf{r}_3) \\ & + H_{\text{hd}}(m_1, m_2, m_3 + m_4, \mathbf{r}_1, \mathbf{r}_3) + H_{\text{hd}}(m_4, m_3, m_1 + m_2, \mathbf{r}_2, \mathbf{r}_3) + H_{\text{hd, cross, bb}}(m_1, m_2, m_3, m_4, \mathbf{r}_1, \mathbf{r}_2, \mathbf{r}_3) \\ & + O\left[\frac{1}{r_3} \left(\frac{r_1}{r_2}\right)^i \left(\frac{r_2}{r_3}\right)^j \left(\frac{r_1}{r_3}\right)^k\right]. \end{aligned} \quad (4)$$

Here, $i + j + k \geq 5$. The various ‘universal’ functions in equation (4) are given by

$$H_{\text{kep}}(m, m', \mathbf{r}, \dot{\mathbf{r}}) = \frac{1}{2} \frac{mm'}{m+m'} \dot{\mathbf{r}}^2 - \frac{Gmm'}{r}; \quad (5a)$$

$$H_{\text{quad}}(m, m', m'', \mathbf{r}, \mathbf{r}') = -\frac{Gmm'm''}{m+m'} \frac{1}{r'} \left(\frac{r}{r'}\right)^2 \frac{1}{2} \left[3(\hat{\mathbf{r}} \cdot \hat{\mathbf{r}}')^2 - 1\right]; \quad (5b)$$

$$H_{\text{oct}}(m, m', m'', \mathbf{r}, \mathbf{r}') = -\frac{Gmm'm''(m-m')}{(m+m')^2} \frac{1}{r'} \left(\frac{r}{r'}\right)^3 \frac{1}{2} \left[5(\hat{\mathbf{r}} \cdot \hat{\mathbf{r}}')^3 - 3(\hat{\mathbf{r}} \cdot \hat{\mathbf{r}}')\right]; \quad (5c)$$

$$H_{\text{hd}}(m, m', m'', \mathbf{r}, \mathbf{r}') = -\frac{Gmm'm''(m^2 - mm' + m'^2)}{(m+m')^3} \frac{1}{r'} \left(\frac{r}{r'}\right)^4 \frac{1}{8} \left[35(\hat{\mathbf{r}} \cdot \hat{\mathbf{r}}')^4 - 30(\hat{\mathbf{r}} \cdot \hat{\mathbf{r}}')^2 + 3\right]; \quad (5d)$$

$$\begin{aligned} H_{\text{hd, cross, bb}}(m_1, m_2, m_3, m_4, \mathbf{r}_1, \mathbf{r}_2, \mathbf{r}_3) = & -\frac{Gm_1 m_2 m_3 m_4}{(m_1 + m_2)(m_3 + m_4)} \frac{1}{r_3} \left(\frac{r_1}{r_3}\right)^2 \left(\frac{r_2}{r_3}\right)^2 \\ & \times \frac{3}{4} \left[1 - 5(\hat{\mathbf{r}}_1 \cdot \hat{\mathbf{r}}_3)^2 - 5(\hat{\mathbf{r}}_2 \cdot \hat{\mathbf{r}}_3)^2 + 35(\hat{\mathbf{r}}_1 \cdot \hat{\mathbf{r}}_3)^2 (\hat{\mathbf{r}}_2 \cdot \hat{\mathbf{r}}_3)^2 + 2(\hat{\mathbf{r}}_1 \cdot \hat{\mathbf{r}}_2)^2 - 20(\hat{\mathbf{r}}_1 \cdot \hat{\mathbf{r}}_2)(\hat{\mathbf{r}}_1 \cdot \hat{\mathbf{r}}_3)(\hat{\mathbf{r}}_2 \cdot \hat{\mathbf{r}}_3)\right]. \end{aligned} \quad (5e)$$

The first three terms in Equation (4) are the Keplerian terms; in the limit that the orbits are described by Keplerian orbits, these terms individually reduce to the constant terms $-G(m+m')/(2a_i)$, where i refers to the corresponding orbit and the masses should be replaced appropriately for each orbit. The other terms in equation (4) give rise to changes to the Keplerian orbits. Note that, as expected, H_{bb} is symmetric with respect to binaries 1 and 2, i.e., it is invariant under the interchange of parameters $m_1 \leftrightarrow m_3$, $m_2 \leftrightarrow m_4$, and $\mathbf{r}_1 \leftrightarrow \mathbf{r}_2$.

It is immediately clear that, to the lowest expansion orders, the quadrupole and octupole orders, $\propto (r/r')^2$ and $\propto (r/r')^3$, respectively, the expanded Hamiltonian is fully described in terms of pairwise interactions only: the interaction between orbit 1 and its outer orbit, and between orbit 2 and its outer orbit. This implies that, up to and including octupole order, any effect of the ‘binarity’ of the companion orbit can only arise from an effect of the companion binarity on the outer orbit, i.e., on \mathbf{r}_3 . This is discussed further below analytically (Section 2.4.1), as well as numerically (Section 3.1).

Only at the ‘hexadecupole’ order, $\propto (r/r')^4$, does there appear a term that involves the properties of three orbits simultaneously, described by $H_{\text{hd, cross, bb}}$. We remark that the latter term contains the factors $(r_1/r_3)^2$ and $(r_2/r_3)^2$ which, individually considered, might suggest that $H_{\text{hd, cross, bb}}$ should be counted as a quadrupole-order term. However, since we assume that both $r_1/r_3 \ll 1$ and $r_2/r_3 \ll 1$, the term $H_{\text{hd, cross, bb}}$ is effectively of fourth order; therefore, we consider it a hexadecupole-order term.

2.2.2 Partial orbit averaging

In the ‘secular’ approximation, one averages the expanded Hamiltonian, equation (4), over some or all orbits. Here, we choose to average over the ‘inner’ orbits, i.e., orbits 1 and 2. This approximation is generally expected to be a good one if $\mathcal{R}_i \ll 1$, where $i \in \{1, 2\}$ refers to orbits 1 and 2, and

$$\mathcal{R}_i = \left[\left(1 + \frac{M_{3-i}}{M_i}\right) \left(\frac{a_i}{Q}\right)^3 (1+E) \right]^{1/2}. \quad (6)$$

If $\mathcal{R}_i \ll 1$ for both $i = 1$ and $i = 2$, the mean motions of both bound orbits are much faster than the angular speed of the para/hyperbolic orbit at periapsis (this consideration is analogous to the binary-single case; see, e.g., equation 1 of Hamers & Samsing 2019a).

4 Hamers & Samsing

The result of the ‘inner’ averaging, written explicitly to the same order as in equation (4), is (see, e.g., Hamers 2018 for a general derivation of the pairwise averaged expressions to any expansion order; the term $\overline{H}_{\text{hex, cross, bb}}$ is derived new here)

$$\begin{aligned} \overline{H}_{\text{bb}} = & \overline{H}_{\text{kep}}(m_1, m_2, a_1) + \overline{H}_{\text{kep}}(m_3, m_4, a_2) + \overline{H}_{\text{kep}}(m_1 + m_2, m_3 + m_4, a_3) \\ & + \overline{H}_{\text{quad}}(m_1, m_2, m_3 + m_4, a_1, \mathbf{e}_1, \mathbf{J}_1, \mathbf{r}_3) + \overline{H}_{\text{quad}}(m_3, m_4, m_1 + m_2, a_2, \mathbf{e}_2, \mathbf{J}_2, \mathbf{r}_3) \\ & + \overline{H}_{\text{oct}}(m_1, m_2, m_3 + m_4, a_1, \mathbf{e}_1, \mathbf{J}_1, \mathbf{r}_3) + \overline{H}_{\text{oct}}(m_3, m_4, m_1 + m_2, a_2, \mathbf{e}_2, \mathbf{J}_2, \mathbf{r}_3) \\ & + \overline{H}_{\text{hex}}(m_1, m_2, m_3 + m_4, a_1, \mathbf{e}_1, \mathbf{J}_1, \mathbf{r}_3) + \overline{H}_{\text{hex}}(m_3, m_4, m_1 + m_2, a_2, \mathbf{e}_2, \mathbf{J}_2, \mathbf{r}_3) + \overline{H}_{\text{hex, cross, bb}}(m_1, m_2, m_3, m_4, a_1, \mathbf{e}_1, \mathbf{J}_1, a_2, \mathbf{e}_2, \mathbf{J}_2, \mathbf{r}_3) \\ & + \mathcal{O} \left[\frac{1}{r_3} \left(\frac{a_1}{a_2} \right)^i \left(\frac{a_2}{r_3} \right)^j \left(\frac{a_1}{r_3} \right)^k \right]. \end{aligned} \quad (7)$$

Here, we defined

$$\overline{H}_{\text{kep}}(m, m', a) \equiv -\frac{Gmm'}{2a}; \quad (8a)$$

$$\overline{H}_{\text{quad}}(m, m', m'', a, \mathbf{e}, \mathbf{J}, \mathbf{r}) \equiv -\frac{Gmm'm''}{m+m'} \frac{1}{r} \left(\frac{a}{r} \right)^2 \frac{1}{4} \left[1 - 6e^2 + 15(\mathbf{e} \cdot \hat{\mathbf{r}})^2 - 3(\mathbf{J} \cdot \hat{\mathbf{r}})^2 \right]; \quad (8b)$$

$$\overline{H}_{\text{oct}}(m, m', m'', a, \mathbf{e}, \mathbf{J}, \mathbf{r}) \equiv -\frac{Gmm'm''}{m+m'} \frac{|m-m'|}{m+m'} \frac{1}{r} \left(\frac{a}{r} \right)^3 \frac{5}{16} (\mathbf{e} \cdot \hat{\mathbf{r}}) \left[3(1-8e^2) + 35(\mathbf{e} \cdot \hat{\mathbf{r}})^2 - 15(\mathbf{J} \cdot \hat{\mathbf{r}})^2 \right]; \quad (8c)$$

$$\begin{aligned} \overline{H}_{\text{hd}}(m, m', m'', a, \mathbf{e}, \mathbf{J}, \mathbf{r}) \equiv & -\frac{Gmm'm''}{m+m'} \frac{m^2 - mm' + m'^2}{m+m'} \frac{1}{r} \left(\frac{a}{r} \right)^4 \frac{3}{64} \left[3 - 20e^2 + 80e^4 + 735(\mathbf{e} \cdot \hat{\mathbf{r}})^4 + 35(\mathbf{J} \cdot \hat{\mathbf{r}})^4 - 10(3 - 10e^2)(\mathbf{J} \cdot \hat{\mathbf{r}})^2 \right. \\ & \left. - 70(\mathbf{e} \cdot \hat{\mathbf{r}})^2 \{ 7(\mathbf{J} \cdot \hat{\mathbf{r}})^2 + 10e^2 - 1 \} \right]; \end{aligned} \quad (8d)$$

$$\begin{aligned} \overline{H}_{\text{hex, cross, bb}}(m_1, m_2, m_3, m_4, a_1, \mathbf{e}_1, \mathbf{J}_1, a_2, \mathbf{e}_2, \mathbf{J}_2, \mathbf{r}) \equiv & -\frac{Gm_1 m_2 m_3 m_4}{(m_1 + m_2)(m_3 + m_4)} \frac{1}{r} \left(\frac{a_1}{r} \right)^2 \left(\frac{a_2}{r} \right)^2 \frac{3}{16} \left[1 - 6e_1^2 - 6e_2^2 + 36e_1^2 e_2^2 + 50(\mathbf{e}_1 \cdot \mathbf{e}_2)^2 \right. \\ & - 10(\mathbf{e}_1 \cdot \mathbf{J}_2)^2 - 10(\mathbf{J}_1 \cdot \mathbf{e}_2)^2 + 2(\mathbf{J}_1 \cdot \mathbf{J}_2)^2 + 25(\mathbf{e}_1 \cdot \hat{\mathbf{r}})^2 + 25(\mathbf{e}_2 \cdot \hat{\mathbf{r}})^2 + 5(6e_2^2 - 1)(\mathbf{J}_1 \cdot \hat{\mathbf{r}})^2 + 5(6e_1^2 - 1)(\mathbf{J}_2 \cdot \hat{\mathbf{r}})^2 \\ & - 150e_2^2(\mathbf{e}_1 \cdot \hat{\mathbf{r}})^2 - 150e_1^2(\mathbf{e}_2 \cdot \hat{\mathbf{r}})^2 - 500(\mathbf{e}_1 \cdot \mathbf{e}_2)(\mathbf{e}_1 \cdot \hat{\mathbf{r}})(\mathbf{e}_2 \cdot \hat{\mathbf{r}}) + 100(\mathbf{J}_1 \cdot \mathbf{e}_2)(\mathbf{J}_1 \cdot \hat{\mathbf{r}})(\mathbf{e}_2 \cdot \hat{\mathbf{r}}) + 100(\mathbf{e}_1 \cdot \mathbf{J}_2)(\mathbf{e}_1 \cdot \hat{\mathbf{r}})(\mathbf{J}_2 \cdot \hat{\mathbf{r}}) \\ & \left. - 20(\mathbf{J}_1 \cdot \mathbf{J}_2)(\mathbf{J}_1 \cdot \hat{\mathbf{r}})(\mathbf{J}_2 \cdot \hat{\mathbf{r}}) - 175(\mathbf{J}_1 \cdot \hat{\mathbf{r}})^2(\mathbf{e}_2 \cdot \hat{\mathbf{r}})^2 - 175(\mathbf{e}_1 \cdot \hat{\mathbf{r}})^2(\mathbf{J}_2 \cdot \hat{\mathbf{r}})^2 + 35(\mathbf{J}_1 \cdot \hat{\mathbf{r}})^2(\mathbf{J}_2 \cdot \hat{\mathbf{r}})^2 + 875(\mathbf{e}_1 \cdot \hat{\mathbf{r}})^2(\mathbf{e}_2 \cdot \hat{\mathbf{r}})^2 \right]. \end{aligned}$$

As should be, the inner-averaged Hamiltonian, equation (7), is still symmetric with respect to orbits 1 and 2.

2.3 Inner-averaged equations of motion

Hamilton’s equations applied to the inner-averaged Hamiltonian equation (2.2.2) imply the following set of equations of motion for the eccentricity \mathbf{e}_i and angular momentum \mathbf{J}_i vectors of orbits 1 and 2, as well as the equation of motion for the outer orbital separation \mathbf{r}_3 :

$$\begin{aligned} \frac{d\mathbf{e}_i}{dt} = & \epsilon_{\text{SA},i}(1 + E \cos \theta) \mathbf{f}_{\dot{\mathbf{e}},\text{quad}}(\mathbf{e}_i, \mathbf{J}_i, \hat{\mathbf{r}}_3) + \epsilon_{\text{SA},i} \epsilon_{\text{oct},i}(1 + E \cos \theta)^2 \mathbf{f}_{\dot{\mathbf{e}},\text{oct}}(\mathbf{e}_i, \mathbf{J}_i, \hat{\mathbf{r}}_3) + \epsilon_{\text{SA},i} \epsilon_{\text{hex},i}(1 + E \cos \theta)^3 \mathbf{f}_{\dot{\mathbf{e}},\text{hex}}(\mathbf{e}_i, \mathbf{J}_i, \hat{\mathbf{r}}_3) \\ & + \epsilon_{\text{SA},i} \epsilon_{\text{hex,cross},i}(1 + E \cos \theta)^3 \mathbf{f}_{\dot{\mathbf{e}},\text{hex,cross}}(\mathbf{e}_i, \mathbf{J}_i, \mathbf{e}_{3-i}, \mathbf{J}_{3-i}, \hat{\mathbf{r}}_3) + \dots; \end{aligned} \quad (9a)$$

$$\begin{aligned} \frac{d\mathbf{J}_i}{dt} = & \epsilon_{\text{SA},i}(1 + E \cos \theta) \mathbf{f}_{\mathbf{J},\text{quad}}(\mathbf{e}_i, \mathbf{J}_i, \hat{\mathbf{r}}_3) + \epsilon_{\text{SA},i} \epsilon_{\text{oct},i}(1 + E \cos \theta)^2 \mathbf{f}_{\mathbf{J},\text{oct}}(\mathbf{e}_i, \mathbf{J}_i, \hat{\mathbf{r}}_3) + \epsilon_{\text{SA},i} \epsilon_{\text{hex},i}(1 + E \cos \theta)^3 \mathbf{f}_{\mathbf{J},\text{hex}}(\mathbf{e}_i, \mathbf{J}_i, \hat{\mathbf{r}}_3) \\ & + \epsilon_{\text{SA},i} \epsilon_{\text{hex,cross},i}(1 + E \cos \theta)^3 \mathbf{f}_{\mathbf{J},\text{hex,cross}}(\mathbf{e}_i, \mathbf{J}_i, \mathbf{e}_{3-i}, \mathbf{J}_{3-i}, \hat{\mathbf{r}}_3) + \dots; \end{aligned} \quad (9b)$$

$$\frac{d^2 \mathbf{r}_3}{dt^2} = -\frac{GM}{r_3^3} \mathbf{r}_3 + \frac{GM}{r_3^2} \mathbf{f}_{\ddot{\mathbf{r}}_3}(m_1, m_2, a_1, \mathbf{e}_1, \mathbf{J}_1, \mathbf{r}_3) + \frac{GM}{r_3^2} \mathbf{f}_{\ddot{\mathbf{r}}_3}(m_3, m_4, a_2, \mathbf{e}_2, \mathbf{J}_2, \mathbf{r}_3) + \dots \quad (9c)$$

Here, ‘...’ denotes higher-order expansion terms, and the auxiliary functions are defined according to

$$\mathbf{f}_{\dot{\mathbf{e}},\text{quad}}(\mathbf{e}, \mathbf{J}, \hat{\mathbf{r}}_3) \equiv \left[-3(\mathbf{J} \times \mathbf{e}) - \frac{3}{2}(\mathbf{J} \cdot \hat{\mathbf{r}}_3)(\mathbf{e} \times \hat{\mathbf{r}}_3) + \frac{15}{2}(\mathbf{e} \cdot \hat{\mathbf{r}}_3)(\mathbf{J} \times \hat{\mathbf{r}}_3) \right]; \quad (10a)$$

$$\mathbf{f}_{\mathbf{J},\text{quad}}(\mathbf{e}, \mathbf{J}, \hat{\mathbf{r}}_3) \equiv \left[-\frac{3}{2}(\mathbf{J} \cdot \hat{\mathbf{r}}_3)(\mathbf{J} \times \hat{\mathbf{r}}_3) + \frac{15}{2}(\mathbf{e} \cdot \hat{\mathbf{r}}_3)(\mathbf{e} \times \hat{\mathbf{r}}_3) \right]; \quad (10b)$$

$$\mathbf{f}_{\dot{\mathbf{e}},\text{oct}}(\mathbf{e}, \mathbf{J}, \hat{\mathbf{r}}_3) \equiv \frac{15}{16} \left[-16(\mathbf{e} \cdot \hat{\mathbf{r}}_3)(\mathbf{J} \times \mathbf{e}) + (1 - 8e^2)(\mathbf{J} \times \hat{\mathbf{r}}_3) - 10(\mathbf{e} \cdot \hat{\mathbf{r}}_3)(\mathbf{J} \cdot \hat{\mathbf{r}}_3)(\mathbf{e} \times \hat{\mathbf{r}}_3) - 5(\mathbf{J} \cdot \hat{\mathbf{r}}_3)^2(\mathbf{J} \times \hat{\mathbf{r}}_3) + 35(\mathbf{e} \cdot \hat{\mathbf{r}}_3)^2(\mathbf{J} \times \hat{\mathbf{r}}_3) \right]; \quad (10c)$$

$$\mathbf{f}_{\dot{\mathbf{e}},\text{oct}}(\mathbf{J}, \mathbf{J}, \hat{\mathbf{r}}_3) \equiv \frac{15}{16} \left[(1 - 8e^2)(\mathbf{e} \times \hat{\mathbf{r}}_3) - 10(\mathbf{e} \cdot \hat{\mathbf{r}}_3)(\mathbf{J} \cdot \hat{\mathbf{r}}_3)(\mathbf{J} \times \hat{\mathbf{r}}_3) - 5(\mathbf{J} \cdot \hat{\mathbf{r}}_3)^2(\mathbf{e} \times \hat{\mathbf{r}}_3) + 35(\mathbf{e} \cdot \hat{\mathbf{r}}_3)^2(\mathbf{e} \times \hat{\mathbf{r}}_3) \right]; \quad (10d)$$

$$\mathbf{f}_{\dot{\mathbf{e}},\text{hex}}(\mathbf{e}, \mathbf{J}, \hat{\mathbf{r}}_3) \equiv \frac{15}{16} \left[7 \left\{ 21(\mathbf{e} \cdot \hat{\mathbf{r}}_3)^3(\mathbf{J} \times \hat{\mathbf{r}}_3) - 7(\mathbf{e} \cdot \hat{\mathbf{r}}_3)^2(\mathbf{J} \cdot \hat{\mathbf{r}}_3)(\mathbf{e} \times \hat{\mathbf{r}}_3) - 7(\mathbf{e} \cdot \hat{\mathbf{r}}_3)(\mathbf{J} \cdot \hat{\mathbf{r}}_3)^2(\mathbf{J} \times \hat{\mathbf{r}}_3) + (\mathbf{J} \cdot \hat{\mathbf{r}}_3)^3(\mathbf{e} \times \hat{\mathbf{r}}_3) \right\} \right]$$

$$+ 7(\mathbf{e} \cdot \hat{\mathbf{r}}_3) \left\{ (\mathbf{J} \times \hat{\mathbf{r}}_3) - 10(\mathbf{e} \cdot \hat{\mathbf{r}}_3)(\mathbf{J} \times \mathbf{e}) - 10e^2(\mathbf{J} \times \hat{\mathbf{r}}_3) \right\} - (3 - 10e^2)(\mathbf{J} \cdot \hat{\mathbf{r}}_3)(\mathbf{e} \times \hat{\mathbf{r}}_3) + 10(\mathbf{J} \cdot \hat{\mathbf{r}}_3)^2(\mathbf{J} \times \mathbf{e}) - 2(1 - 8e^2)(\mathbf{J} \times \mathbf{e}) \Big]; \quad (10e)$$

$$f_{\mathbf{j}, \text{hex}}(\mathbf{e}, \mathbf{J}, \hat{\mathbf{r}}_3) \equiv \frac{15}{16} \left[7 \left\{ 1 - 10e^2 + 21(\mathbf{e} \cdot \hat{\mathbf{r}}_3)^2 - 7(\mathbf{J} \cdot \hat{\mathbf{r}}_3)^2 \right\} (\mathbf{e} \cdot \hat{\mathbf{r}}_3)(\mathbf{e} \times \hat{\mathbf{r}}_3) + \left\{ -3 + 10e^2 - 49(\mathbf{e} \cdot \hat{\mathbf{r}}_3)^2 + 7(\mathbf{J} \cdot \hat{\mathbf{r}}_3)^2 \right\} (\mathbf{J} \cdot \hat{\mathbf{r}}_3)(\mathbf{J} \times \hat{\mathbf{r}}_3) \right]; \quad (10f)$$

$$f_{\mathbf{e}, \text{hex}, \text{cross}}(\mathbf{e}_i, \mathbf{J}_i, \mathbf{e}_{3-i}, \mathbf{J}_{3-i}, \hat{\mathbf{r}}_3) \equiv \frac{3}{16} \left[-20(\mathbf{J}_i \cdot \mathbf{e}_{3-i})(\mathbf{e}_i \times \mathbf{e}_{3-i}) + 4(\mathbf{J}_i \cdot \mathbf{J}_{3-i})(\mathbf{e}_i \times \mathbf{J}_{3-i}) + 10(6e_{3-i}^2 - 1)(\mathbf{J}_i \cdot \hat{\mathbf{r}}_3)(\mathbf{e}_i \times \hat{\mathbf{r}}_3) \right. \\ \left. - 20(\mathbf{J}_{3-i} \cdot \hat{\mathbf{r}}_3) [(\mathbf{J}_i \cdot \hat{\mathbf{r}}_3)(\mathbf{e}_i \times \mathbf{J}_{3-i}) + (\mathbf{J}_i \cdot \mathbf{J}_{3-i})(\mathbf{e}_i \times \hat{\mathbf{r}}_3)] + 100(\mathbf{e}_{3-i} \cdot \hat{\mathbf{r}}_3) [(\mathbf{J}_i \cdot \hat{\mathbf{r}}_3)(\mathbf{e}_i \times \mathbf{e}_{3-i}) + (\mathbf{J}_i \cdot \mathbf{e}_{3-i})(\mathbf{e}_i \times \hat{\mathbf{r}}_3)] \right. \\ \left. + 70(\mathbf{J}_i \cdot \hat{\mathbf{r}}_3)(\mathbf{J}_{3-i} \cdot \hat{\mathbf{r}}_3)^2(\mathbf{e}_i \times \hat{\mathbf{r}}_3) - 350(\mathbf{J}_i \cdot \hat{\mathbf{r}}_3)(\mathbf{e}_{3-i} \cdot \hat{\mathbf{r}}_3)^2(\mathbf{e}_i \times \hat{\mathbf{r}}_3) - 12(\mathbf{J}_i \times \mathbf{e}_i) + 72e_{3-i}^2(\mathbf{J}_i \times \mathbf{e}_i) + 100(\mathbf{e}_i \cdot \mathbf{e}_{3-i})(\mathbf{J}_i \times \mathbf{e}_{3-i}) \right. \\ \left. - 20(\mathbf{e}_i \cdot \mathbf{J}_{3-i})(\mathbf{J}_i \times \mathbf{J}_{3-i}) + 50(\mathbf{e}_i \cdot \hat{\mathbf{r}}_3)(\mathbf{J}_i \times \hat{\mathbf{r}}_3) + 60(\mathbf{J}_{3-i} \cdot \hat{\mathbf{r}}_3)^2(\mathbf{J}_i \times \mathbf{e}_i) - 300e_{3-i}^2(\mathbf{e}_i \cdot \hat{\mathbf{r}}_3)(\mathbf{J}_i \times \hat{\mathbf{r}}_3) - 300(\mathbf{e}_{3-i} \cdot \hat{\mathbf{r}}_3)^2(\mathbf{J}_i \times \mathbf{e}_i) \right. \\ \left. - 500(\mathbf{e}_{3-i} \cdot \hat{\mathbf{r}}_3) [(\mathbf{e}_i \cdot \hat{\mathbf{r}}_3)(\mathbf{J}_i \times \mathbf{e}_{3-i}) + (\mathbf{e}_i \cdot \mathbf{e}_{3-i})(\mathbf{J}_i \times \hat{\mathbf{r}}_3)] + 100(\mathbf{J}_{3-i} \cdot \hat{\mathbf{r}}_3) [(\mathbf{e}_i \cdot \hat{\mathbf{r}}_3)(\mathbf{J}_i \times \mathbf{J}_{3-i}) + (\mathbf{e}_i \cdot \mathbf{J}_{3-i})(\mathbf{J}_i \times \hat{\mathbf{r}}_3)] \right. \\ \left. + 1750(\mathbf{e}_i \cdot \hat{\mathbf{r}}_3)(\mathbf{e}_{3-i} \cdot \hat{\mathbf{r}}_3)^2(\mathbf{J}_i \times \hat{\mathbf{r}}_3) - 350(\mathbf{e}_i \cdot \hat{\mathbf{r}}_3)(\mathbf{J}_{3-i} \cdot \hat{\mathbf{r}}_3)^2(\mathbf{J}_i \times \hat{\mathbf{r}}_3) \right];$$

$$f_{\mathbf{j}, \text{hex}, \text{cross}}(\mathbf{e}_i, \mathbf{J}_i, \mathbf{e}_{3-i}, \mathbf{J}_{3-i}, \hat{\mathbf{r}}_3) \equiv \frac{3}{16} \left[100(\mathbf{e}_i \cdot \mathbf{e}_{3-i})(\mathbf{e}_i \times \mathbf{e}_{3-i}) - 20(\mathbf{e}_i \cdot \mathbf{J}_{3-i})(\mathbf{e}_i \times \mathbf{J}_{3-i}) + 50(\mathbf{e}_i \cdot \hat{\mathbf{r}}_3)(\mathbf{e}_i \times \hat{\mathbf{r}}_3) \right. \\ \left. - 300e_{3-i}^2(\mathbf{e}_i \cdot \hat{\mathbf{r}}_3)(\mathbf{e}_i \times \hat{\mathbf{r}}_3) - 500(\mathbf{e}_i \cdot \hat{\mathbf{r}}_3) [(\mathbf{e}_i \cdot \hat{\mathbf{r}}_3)(\mathbf{e}_i \times \mathbf{e}_{3-i}) + (\mathbf{e}_i \cdot \mathbf{e}_{3-i})(\mathbf{e}_i \times \hat{\mathbf{r}}_3)] + 100(\mathbf{J}_{3-i} \cdot \hat{\mathbf{r}}_3) [(\mathbf{e}_i \cdot \hat{\mathbf{r}}_3)(\mathbf{e}_i \times \mathbf{J}_{3-i}) \right. \\ \left. + (\mathbf{e}_i \cdot \mathbf{J}_{3-i})(\mathbf{e}_i \times \hat{\mathbf{r}}_3)] + 1750(\mathbf{e}_i \cdot \hat{\mathbf{r}}_3)(\mathbf{e}_{3-i} \cdot \hat{\mathbf{r}}_3)^2(\mathbf{e}_i \times \hat{\mathbf{r}}_3) - 350(\mathbf{e}_i \cdot \hat{\mathbf{r}}_3)(\mathbf{J}_{3-i} \cdot \hat{\mathbf{r}}_3)^2(\mathbf{e}_i \times \hat{\mathbf{r}}_3) - 20(\mathbf{J}_i \cdot \mathbf{e}_{3-i})(\mathbf{J}_i \times \mathbf{e}_{3-i}) \right. \\ \left. + 4(\mathbf{J}_i \cdot \mathbf{J}_{3-i})(\mathbf{J}_i \times \mathbf{J}_{3-i}) + 10(6e_{3-i}^2 - 1)(\mathbf{J}_i \cdot \hat{\mathbf{r}}_3)(\mathbf{J}_i \times \hat{\mathbf{r}}_3) - 20(\mathbf{J}_{3-i} \cdot \hat{\mathbf{r}}_3) [(\mathbf{J}_i \cdot \hat{\mathbf{r}}_3)(\mathbf{J}_i \times \mathbf{J}_{3-i}) + (\mathbf{J}_i \cdot \mathbf{J}_{3-i})(\mathbf{J}_i \times \hat{\mathbf{r}}_3)] \right. \\ \left. + 100(\mathbf{e}_{3-i} \cdot \hat{\mathbf{r}}_3) [(\mathbf{J}_i \cdot \hat{\mathbf{r}}_3)(\mathbf{J}_i \times \mathbf{e}_{3-i}) + (\mathbf{J}_i \cdot \mathbf{e}_{3-i})(\mathbf{J}_i \times \hat{\mathbf{r}}_3)] + 70(\mathbf{J}_i \cdot \hat{\mathbf{r}}_3)(\mathbf{J}_{3-i} \cdot \hat{\mathbf{r}}_3)^2(\mathbf{J}_i \times \hat{\mathbf{r}}_3) - 350(\mathbf{J}_i \cdot \hat{\mathbf{r}}_3)(\mathbf{e}_{3-i} \cdot \hat{\mathbf{r}}_3)^2(\mathbf{J}_i \times \hat{\mathbf{r}}_3) \right]; \quad (10g)$$

$$f_{\hat{\mathbf{r}}_3}(m, m', a, \mathbf{e}, \mathbf{J}, \mathbf{r}_3) = \frac{mm'}{m+m'} \left(\frac{a}{r_3} \right)^2 \frac{1}{4} \left[-3(1 - 6e^2)\hat{\mathbf{r}}_3 + 30(\mathbf{e} \cdot \hat{\mathbf{r}}_3)\mathbf{e} - 75(\mathbf{e} \cdot \hat{\mathbf{r}}_3)^2\hat{\mathbf{r}}_3 - 6(\mathbf{J} \cdot \hat{\mathbf{r}}_3)\mathbf{J} + 15(\mathbf{J} \cdot \hat{\mathbf{r}}_3)^2\hat{\mathbf{r}}_3 \right]. \quad (10h)$$

Other (dimensionless) parameters appearing in equation (9) are defined according to

$$\epsilon_{\text{SA}, i} \equiv \left[\frac{M_{3-i}^2}{M_i M} \left(\frac{a_i}{Q} \right)^3 (1 + E)^{-3} \right]^{1/2}; \quad (11a)$$

$$\epsilon_{\text{oct}, i} \equiv \frac{|m_{i,A} - m_{i,B}|}{M_i} \frac{a_i}{Q} \frac{1}{1 + E}; \quad (11b)$$

$$\epsilon_{\text{hex}, i} \equiv \frac{m_{i,A}^2 - m_{i,A}m_{i,B} + m_{i,B}^2}{M_i^2} \left(\frac{a_i}{Q} \right)^2 \frac{1}{(1 + E)^2}; \quad (11c)$$

$$\epsilon_{\text{hex}, \text{cross}, i} = \frac{m_{3-i,A}m_{3-i,B}}{M_{3-i}^2} \left(\frac{a_{3-i}}{Q} \right)^2 \frac{1}{(1 + E)^2}. \quad (11d)$$

Here, $m_{i,A} = m_1$ and $m_{i,B} = m_2$ if $i = 1$, and $m_{i,A} = m_3$ and $m_{i,B} = m_4$ if $i = 2$. For future convenience (Section 2.4 below), we formulated the equations of motion for \mathbf{e}_i and \mathbf{J}_i in terms of θ , the true anomaly of the outer orbit, which is related to the physical time according to equation (2). Note that in the latter equation and in the inner-averaged approximation, E and a_3 are allowed to vary and are determined by the equation for \mathbf{r}_3 , equation (9c).

2.4 Approximate analytic expressions for the eccentricity and angular-momentum changes

2.4.1 Outer orbit

We first consider the backreaction of the outer orbit on the quadrupole moment of the inner two binaries. This effect is described by Equation (9c) to quadrupole expansion order (since the backreaction effect turns out to be small even at lowest order, we will not consider it at higher orders). We can get an approximate expression for the outer orbital changes (Δa_3 , Δe_3 , and Δi_3) by substituting the solution to equation (9c) in the absence of the perturbation terms $\propto f_{\hat{\mathbf{r}}_3}$ (i.e., the solution if $\ddot{\mathbf{r}}_3 = -GM/r_3^3\mathbf{r}_3$, resulting in purely Keplerian motion), into the perturbation terms and integrating the subsequent expressions over the outer orbit. Let the perturbation term to the Keplerian acceleration be denoted as

$$\mathbf{f}_3 \equiv \frac{GM}{r_3^2} \mathbf{f}_{\hat{\mathbf{r}}_3}(m_1, m_2, a_1, \mathbf{e}_1, \mathbf{J}_1, \mathbf{r}_3) + \frac{GM}{r_3^2} \mathbf{f}_{\hat{\mathbf{r}}_3}(m_3, m_4, a_2, \mathbf{e}_2, \mathbf{J}_2, \mathbf{r}_3). \quad (12)$$

6 Hamers & Samsing

The changes to the outer semimajor axis, eccentricity vector, and (specific) angular-momentum vector ($\mathbf{h}_3 \equiv \mathbf{r}_3 \times \dot{\mathbf{r}}_3$) can then be found according to (e.g., Eggleton 2006, appendix C)

$$\frac{\Delta a_3}{a_3} = \int_{-L}^L d\theta \frac{-2a_3}{GM_1 M_2} (-\dot{\mathbf{r}}_3 \cdot \mathbf{f}_3) \frac{dt}{d\theta} = 0; \quad (13a)$$

$$\Delta \mathbf{e}_3 = \int_{-L}^L d\theta \frac{1}{GM} [2\mathbf{r}_3 (\dot{\mathbf{r}}_3 \cdot \mathbf{f}_3) - \mathbf{f}_3 (\mathbf{r}_3 \cdot \dot{\mathbf{r}}_3) - \dot{\mathbf{r}}_3 (\mathbf{r}_3 \cdot \mathbf{f}_3)] \frac{dt}{d\theta} = \mathbf{f}_{\Delta \mathbf{e}_3}(m_1, m_2, a_1, \mathbf{e}_1, J_1, E) + \mathbf{f}_{\Delta \mathbf{e}_3}(m_3, m_4, a_2, \mathbf{e}_2, J_2, E); \quad (13b)$$

$$\Delta \mathbf{h}_3/h_3 = \int_{-L}^L d\theta \frac{1}{h_3} (\mathbf{r}_3 \times \mathbf{f}_3) \frac{dt}{d\theta} = \mathbf{f}_{\Delta \mathbf{h}_3}(m_1, m_2, a_1, \mathbf{e}_1, J_1, E) + \mathbf{f}_{\Delta \mathbf{h}_3}(m_3, m_4, a_2, \mathbf{e}_2, J_2, E). \quad (13c)$$

Here, we defined the additional expressions

$$\begin{aligned} \mathbf{f}_{\Delta \mathbf{e}_3}(m, m', a, \mathbf{e}, J, E) \equiv & \frac{mm'}{(m+m')^2} \left(\frac{a}{Q} \right)^2 \left[\frac{(E-1)^{5/2} \sqrt{E+1}}{E^3} (5e_x e_y - J_x J_y) \hat{\mathbf{x}} + \frac{3}{32(E+1)^2} \left\{ \frac{8\sqrt{E^2-1}}{3E^3} \left(4E^4 (1+4e_x^2 - e_y^2 - 6e_z^2 \right. \right. \right. \\ & \left. \left. \left. - 2J_x^2 - J_y^2 \right) + E^2 (2 - 17e_x^2 + 23e_y^2 - 12e_z^2 + J_x^2 - 7J_y^2) + 2 (5e_x^2 - 5e_y^2 - J_x^2 + J_y^2) \right\} + 8EL (2 + 3e_x^2 + 3e_y^2 - 12e_z^2 - 3J_x^2 - 3J_y^2) \right] \hat{\mathbf{y}} \\ & - \frac{\sqrt{E^2-1} (2E^2+1) + 3E^2 L}{2E(E+1)^2} (5e_y e_z - J_y J_z) \hat{\mathbf{z}}; \end{aligned} \quad (14a)$$

$$\begin{aligned} \mathbf{f}_{\Delta \mathbf{h}_3}(m, m', a, \mathbf{e}, J, E) \equiv & \frac{mm'}{(m+m')^2} \left(\frac{a}{Q} \right)^2 \left[\frac{\sqrt{1-\frac{1}{E^2}} (2E^2+1) + 3EL}{2E(E+1)^2} (5e_y e_z - J_y J_z) \hat{\mathbf{x}} - \frac{\sqrt{1-\frac{1}{E^2}} (4E^2-1) + 3EL}{2E(E+1)^2} (5e_x e_z - J_x J_z) \hat{\mathbf{y}} \right. \\ & \left. + \frac{(E-1)^{3/2}}{E^2 \sqrt{E+1}} (5e_x e_y - J_x J_y) \hat{\mathbf{z}} \right]. \end{aligned} \quad (14b)$$

Since $\hat{\mathbf{e}}_3 = \hat{\mathbf{x}}$ initially, for small perturbations, the scalar eccentricity change is given by

$$\Delta e_3 \simeq \hat{\mathbf{e}}_3 \cdot \Delta \mathbf{e}_3 = \frac{(E-1)^{5/2} \sqrt{E+1}}{E^3} \left[\frac{m_1 m_2}{M_1^2} \left(\frac{a_1}{Q} \right)^2 (5e_{1,x} e_{1,y} - J_{1,x} J_{1,y}) + \frac{m_3 m_4}{M_2^2} \left(\frac{a_2}{Q} \right)^2 (5e_{2,x} e_{2,y} - J_{2,x} J_{2,y}) \right]. \quad (15)$$

Note that $\Delta e_3 = 0$ if $E = 1$ (parabolic orbits), and becomes independent of E as $E \gg 1$.

The inclination change, Δi_3 , is obtained from the new $\mathbf{h}'_3 = h_3 \hat{\mathbf{z}} + \Delta \mathbf{h}_3$ and noting that the inclination is measured with respect to the z -axis, giving

$$\begin{aligned} \cos \Delta i_3 = & \frac{1 + \frac{\mathbf{h}_3 \cdot \hat{\mathbf{z}}}{h_3}}{\left\| \hat{\mathbf{z}} + \frac{\Delta \mathbf{h}_3}{h_3} \right\|} = 2E \left[a_1^2 (E-1)^{3/2} m_1 m_2 M_2^2 (5e_{1,x} e_{1,y} - J_{1,x} J_{1,y}) + a_2^2 (E-1)^{3/2} m_3 m_4 M_1^2 (5e_{2,x} e_{2,y} - J_{2,x} J_{2,y}) + E^2 \sqrt{E+1} M_1^2 M_2^2 Q^2 \right] \\ & \times (1-E^2)^{-3/2} \left[4Q^3 (1-E^2)^3 \left(\sqrt{\frac{(E-1)^3 E^2}{Q^3}} (a_1^2 m_1 m_2 M_2^2 (5e_{1,x} e_{1,y} - J_{1,x} J_{1,y}) + a_2^2 m_3 m_4 M_1^2 (5e_{2,x} e_{2,y} - J_{2,x} J_{2,y})) \right. \right. \\ & \left. \left. + E^3 M_1^2 M_2^2 \sqrt{(E+1)Q} \right)^2 + (1-E)^3 E^4 \left(\sqrt{1-\frac{1}{E^2}} (4E^2-1) + 3EL \right)^2 (a_1^2 m_1 m_2 M_2^2 (5e_{1,x} e_{1,z} - J_{1,x} J_{1,z}) \right. \right. \\ & \left. \left. + a_2^2 m_3 m_4 M_1^2 (5e_{2,x} e_{2,z} - J_{2,x} J_{2,z}) \right)^2 + (1-E)^3 E^4 \left(\sqrt{1-\frac{1}{E^2}} (2E^2+1) + 3EL \right)^2 (a_1^2 m_1 m_2 M_2^2 (5e_{1,y} e_{1,z} - J_{1,y} J_{1,z}) \right. \right. \\ & \left. \left. + a_2^2 m_3 m_4 M_1^2 (5e_{2,y} e_{2,z} - J_{2,y} J_{2,z}) \right)^2 \right]^{-1/2}. \end{aligned} \quad (16)$$

Here, we used that the initial $h_3 = \sqrt{GMQ(1+E)}$.

From these equations for Δe_3 and Δi_3 , it is clear that the backreaction effects scale with $(a_i/Q)^2$ and so are typically small. This is also borne out by numerical simulations below (Section 3).

2.4.2 Inner orbits

We can obtain approximate expressions for the scalar eccentricity change of orbit i ($i \in \{1, 2\}$) by integrating the equations of motion, equation (9), over θ assuming that all orbits (including the outer orbit) are static (i.e., constant \mathbf{e}_i and J_i). The result is

$$\Delta e_i = \Delta e_{i,\text{quad}} + \Delta e_{i,\text{oct}} + \Delta e_{i,\text{hex}} + \Delta e_{i,\text{hex,cross}} \quad (17)$$

where

$$\Delta e_{i,\text{quad}} = \epsilon_{\text{SA},i} \frac{5}{2e_i E} \left(\sqrt{1 - \frac{1}{E^2}} \left(2e_{i,x} e_{i,y} (E^2 - 1) J_{i,z} + e_{i,x} e_{i,z} (1 - 4E^2) J_{i,y} + e_{i,y} e_{i,z} (2E^2 + 1) J_{i,x} \right) + 3e_{i,z} E L(e_{i,y} J_{i,x} - e_{i,x} J_{i,y}) \right); \quad (18a)$$

$$\begin{aligned} \Delta e_{i,\text{oct}} = \epsilon_{\text{SA},i} \epsilon_{\text{oct},i} \frac{5}{32e_i E^2} & \left[3E^3 L \left(e_{i,x}^2 (3e_{i,y} J_{i,z} - 73e_{i,z} J_{i,y}) + 10e_{i,x} J_{i,x} (7e_{i,y} e_{i,z} + J_{i,y} J_{i,z}) \right. \right. \\ & + e_{i,z} J_{i,y} \left(-3e_{i,y}^2 + 5J_{i,x}^2 + 5J_{i,y}^2 - 4 \right) + e_{i,y} J_{i,z} \left(3e_{i,y}^2 - 15J_{i,x}^2 - 5J_{i,y}^2 + 4 \right) - 32e_{i,y} e_{i,z}^2 J_{i,z} + 32e_{i,z}^3 J_{i,y} \\ & + \sqrt{1 - \frac{1}{E^2}} \left(-e_{i,x}^2 \left(e_{i,z} (160E^4 + 45E^2 + 14) J_{i,y} - 3e_{i,y} (16E^4 - 27E^2 + 14) J_{i,z} \right) \right. \\ & + 2e_{i,x} \left(8E^4 + 9E^2 - 2 \right) J_{i,x} (7e_{i,y} e_{i,z} + J_{i,y} J_{i,z}) + e_{i,y}^3 \left(-8E^4 + 31E^2 - 14 \right) J_{i,z} + e_{i,y}^2 e_{i,z} \left(8E^4 - 31E^2 + 14 \right) J_{i,y} \\ & - e_{i,y} J_{i,z} \left(8E^4 (8e_{i,z}^2 + 4J_{i,x}^2 + J_{i,y}^2 - 1) + E^2 (32e_{i,z}^2 + 11J_{i,x}^2 + 9J_{i,y}^2 - 4) + 2(J_{i,x}^2 - J_{i,y}^2) \right) \\ & \left. \left. + e_{i,z} J_{i,y} \left(8E^4 (8e_{i,z}^2 + 2J_{i,x}^2 + J_{i,y}^2 - 1) + E^2 (32e_{i,z}^2 - 7J_{i,x}^2 + 9J_{i,y}^2 - 4) + 6J_{i,x}^2 - 2J_{i,y}^2 \right) \right) \right]; \quad (18b) \end{aligned}$$

$$\begin{aligned} \Delta e_{i,\text{hex}} = \epsilon_{\text{SA},i} \epsilon_{\text{hex},i} \frac{7}{128e_i E^3} & \left[15E^3 L \left(e_{i,y} \left(e_{i,z} J_{i,x} \left(e_{i,x}^2 (129E^2 + 46) + E^2 (-21J_{i,x}^2 + 21J_{i,y}^2 + 6) - 2(7J_{i,x}^2 + 7J_{i,y}^2 - 4) \right) \right. \right. \\ & + 2e_{i,x} J_{i,z} \left(3E^2 (e_{i,x}^2 - 14J_{i,x}^2 + 2) + 14(J_{i,y}^2 - J_{i,x}^2) \right) - 120e_{i,x} e_{i,z}^2 E^2 J_{i,z} - 20e_{i,x}^3 (3E^2 + 4) J_{i,x} \\ & + e_{i,x} J_{i,y} \left(e_{i,z} \left(e_{i,x}^2 (-135E^2 + 46) \right) + 3E^2 (21J_{i,x}^2 + 7J_{i,y}^2 - 6) + 2(7J_{i,x}^2 + 7J_{i,y}^2 - 4) \right) + 14e_{i,x} (3E^2 + 2) J_{i,x} J_{i,z} \\ & + 20e_{i,z}^3 (9E^2 + 4) \left. \right) + e_{i,y}^3 \left(6e_{i,x} E^2 J_{i,z} + e_{i,z} (3E^2 + 46) J_{i,x} \right) - e_{i,y}^2 e_{i,z} \left(e_{i,x} e_{i,z} (9E^2 + 46) + 14(3E^2 + 2) J_{i,x} J_{i,z} \right) \\ & + \sqrt{1 - \frac{1}{E^2}} \left(e_{i,x}^3 \left(6e_{i,y} (32E^6 - 63E^4 + 70E^2 - 24) J_{i,z} + e_{i,z} (-1024E^6 - 1751E^4 + 24E^2 + 36) J_{i,y} \right) \right. \\ & + e_{i,x}^2 J_{i,x} \left(e_{i,y} e_{i,z} (832E^6 + 2129E^4 - 444E^2 + 108) + 2(128E^6 + 421E^4 - 36E^2 + 12) J_{i,y} J_{i,z} \right) \\ & + e_{i,x} \left(-6e_{i,y}^3 (16E^6 - 81E^4 + 74E^2 - 24) J_{i,z} + e_{i,y}^2 e_{i,z} (128E^6 - 1049E^4 + 204E^2 - 108) J_{i,y} \right. \\ & - 4e_{i,y} J_{i,z} \left(8E^6 (30e_{i,z}^2 + 20J_{i,x}^2 + J_{i,y}^2 - 3) + E^4 (270e_{i,z}^2 + 269J_{i,x}^2 - 80J_{i,y}^2 - 27) - 3E^2 (20e_{i,z}^2 + J_{i,x}^2 + 13J_{i,y}^2 - 2) - 6J_{i,x}^2 + 6J_{i,y}^2 \right) \\ & + e_{i,z} J_{i,y} \left(128E^6 (10e_{i,z}^2 + 4J_{i,x}^2 + J_{i,y}^2 - 1) + E^4 (2740e_{i,z}^2 + 655J_{i,x}^2 + 421J_{i,y}^2 - 274) - 12E^2 (10e_{i,z}^2 - 2J_{i,x}^2 + 3J_{i,y}^2 - 1) \right. \\ & + 12(J_{i,y}^2 - 3J_{i,x}^2) \left. \right) - e_{i,y} J_{i,x} \left(e_{i,y}^2 e_{i,z} (32E^6 - 563E^4 - 240E^2 + 36) + 2e_{i,y} (128E^6 + 421E^4 - 36E^2 + 12) J_{i,y} J_{i,z} \right. \\ & + e_{i,z} \left(32E^6 (10e_{i,z}^2 + 4J_{i,x}^2 - 5J_{i,y}^2 - 1) + E^4 (1660e_{i,z}^2 + 421J_{i,x}^2 - 101J_{i,y}^2 - 166) + 12E^2 (10e_{i,z}^2 - 3J_{i,x}^2 + 16J_{i,y}^2 - 1) \right. \\ & \left. \left. + 12(J_{i,x}^2 - 3J_{i,y}^2) \right) \right) \right]; \quad (18c) \end{aligned}$$

$$\begin{aligned} \Delta e_{i,\text{hex,cross}} = \epsilon_{\text{SA},i} \epsilon_{\text{hex,cross},i} \frac{5}{64e_i E^3} & \left[3 \left(-6(5e_{3-i,x} (2e_{3-i,z} (11E^2 + 4) J_{i,y} + e_{3-i,y} (3E^2 + 2) J_{i,z}) - J_{3-i,x} ((3E^2 + 2) J_{i,z} J_{3-i,y} \right. \right. \\ & + 2(11E^2 + 4) J_{i,y} J_{3-i,z}) \left. \right) e_{i,x}^2 + e_{i,z} \left(-5(105E^2 + 34) J_{i,y} e_{3-i,x}^2 + 30e_{3-i,y} (3E^2 + 2) J_{i,x} e_{3-i,x} + 60e_{3-i,y} e_{3-i,z} (E^2 + 4) J_{i,z} \right. \\ & - 6J_{3-i,y} \left((3E^2 + 2) J_{i,x} J_{3-i,x} + 2(E^2 + 4) J_{i,z} J_{3-i,z} \right) + J_{i,y} \left(5(3E^2 - 22) e_{3-i,y}^2 - 90E^2 + 213E^2 J_{3-i,x}^2 + 82J_{3-i,x}^2 + 105E^2 J_{3-i,y}^2 \right. \\ & + 70J_{3-i,y}^2 - 48E^2 J_{3-i,z}^2 - 32J_{3-i,z}^2 + 20e_{3-i,z}^2 (39E^2 + 20) - 40 \left. \right) e_{i,x} + 12e_{i,z}^2 \left(-5e_{3-i,y} e_{3-i,z} (E^2 + 4) J_{i,x} + (E^2 + 4) J_{3-i,y} J_{3-i,z} J_{i,x} \right. \\ & + 5e_{3-i,x} e_{3-i,z} (11E^2 + 4) J_{i,y} - (11E^2 + 4) J_{i,y} J_{3-i,x} J_{3-i,z} + 6e_{i,y}^2 \left(5e_{3-i,y} (2e_{3-i,z} (E^2 + 4) J_{i,x} + e_{3-i,x} (3E^2 + 2) J_{i,z}) \right. \\ & - J_{3-i,y} \left((3E^2 + 2) J_{i,z} J_{3-i,x} + 2(E^2 + 4) J_{i,x} J_{3-i,z} \right) \left. \right) + e_{i,y} \left(12e_{i,x} \left(5(3J_{i,z} E^2 + J_{i,z}) e_{3-i,x}^2 + 5e_{3-i,z} (11E^2 + 4) J_{i,x} e_{3-i,x} \right. \right. \\ & - 9E^2 J_{i,z} J_{3-i,x}^2 - J_{i,z} J_{3-i,x}^2 - 6E^2 J_{i,z} J_{3-i,y}^2 + J_{i,z} J_{3-i,y}^2 - 5e_{3-i,y} e_{3-i,z} (E^2 + 4) J_{i,y} - 5e_{3-i,y}^2 J_{i,z} - 30e_{3-i,z}^2 E^2 J_{i,z} + 5E^2 J_{i,z} \\ & - 11E^2 J_{i,x} J_{3-i,x} J_{3-i,z} - 4J_{i,x} J_{3-i,x} J_{3-i,z} + E^2 J_{i,y} J_{3-i,y} J_{3-i,z} + 4J_{i,y} J_{3-i,y} J_{3-i,z} \left. \right) + e_{i,z} \left(-30e_{3-i,x} (e_{3-i,y} (3E^2 + 2) J_{i,y} \right. \\ & \left. + 2e_{3-i,z} (11E^2 + 4) J_{i,z}) + 6J_{3-i,x} \left((3E^2 + 2) J_{i,y} J_{3-i,y} + 2(11E^2 + 4) J_{i,z} J_{3-i,z} \right) + J_{i,x} \left(5(69E^2 + 22) e_{3-i,x}^2 - 400e_{3-i,z}^2 \right. \right. \end{aligned}$$

$$\begin{aligned}
& -420e_{3-i,z}^2 E^2 + 30E^2 - 105E^2 J_{3-i,x}^2 - 70J_{3-i,x}^2 - 33E^2 J_{3-i,y}^2 - 82J_{3-i,y}^2 + 48E^2 J_{3-i,z}^2 + 32J_{3-i,z}^2 - 5e_{3-i,y}^2 (3E^2 - 34) + 40) \Big) \Big) LE^3 \\
& + \sqrt{1 - \frac{1}{E^2}} \left\{ -6 \left(5e_{3-i,x} \left(2e_{3-i,z} \left(16E^4 + 31E^2 - 2 \right) J_{i,y} E^2 + e_{3-i,y} \left(23E^4 - 12E^2 + 4 \right) J_{i,z} \right) - J_{3-i,x} \left(2 \left(16E^4 + 31E^2 - 2 \right) J_{i,y} J_{3-i,z} E^2 \right. \right. \right. \\
& + \left. \left. \left(23E^4 - 12E^2 + 4 \right) J_{i,z} J_{3-i,y} \right) \right) e_{i,x}^2 + e_{i,z} \left(320J_{i,y} J_{3-i,x}^2 E^6 + 128J_{i,y} J_{3-i,y}^2 E^6 - 64J_{i,y} J_{3-i,z}^2 E^6 + 1088e_{3-i,z}^2 J_{i,y} E^6 - 128J_{i,y} E^6 \right. \\
& + 577J_{i,y} J_{3-i,x}^2 E^4 + 421J_{i,y} J_{3-i,y}^2 E^4 - 176J_{i,y} J_{3-i,z}^2 E^4 + 2524e_{3-i,z}^2 J_{i,y} E^4 - 274J_{i,y} E^4 - 138J_{i,x} J_{3-i,x} J_{3-i,y} E^4 - 156J_{i,z} J_{3-i,y} J_{3-i,z} E^4 \\
& - 36J_{i,y} J_{3-i,y}^2 E^2 - 72e_{3-i,z}^2 J_{i,y} E^2 + 12J_{i,y} E^2 + 60e_{3-i,y} e_{3-i,z} \left(13E^2 + 2 \right) J_{i,z} E^2 + 72J_{i,x} J_{3-i,x} J_{3-i,y} E^2 - 24J_{i,z} J_{3-i,y} J_{3-i,z} E^2 \\
& - 12J_{i,y} J_{3-i,x}^2 + 12J_{i,y} J_{3-i,y}^2 + 30e_{3-i,x} e_{3-i,y} \left(23E^4 - 12E^2 + 4 \right) J_{i,x} + e_{3-i,y}^2 \left(128E^6 - 461E^4 + 108E^2 - 60 \right) J_{i,y} \\
& - e_{3-i,x}^2 \left(832E^6 + 1241E^4 + 72E^2 - 60 \right) J_{i,y} - 24J_{i,x} J_{3-i,x} J_{3-i,y} \left) e_{i,x} + 12e_{i,z}^2 E^2 \left(-5e_{3-i,y} e_{3-i,z} \left(13E^2 + 2 \right) J_{i,x} \right. \right. \\
& + \left. \left. \left(13E^2 + 2 \right) J_{3-i,y} J_{3-i,z} J_{i,x} + 5e_{3-i,x} e_{3-i,z} \left(16E^4 + 31E^2 - 2 \right) J_{i,y} + \left(-16E^4 - 31E^2 + 2 \right) J_{i,y} J_{3-i,x} J_{3-i,z} \right) \right. \\
& + 6e_{i,y}^2 \left(5e_{3-i,y} \left(2e_{3-i,z} \left(13E^2 + 2 \right) J_{i,x} E^2 + e_{3-i,x} \left(23E^4 - 12E^2 + 4 \right) J_{i,z} \right) - J_{3-i,y} \left(2 \left(13E^2 + 2 \right) J_{i,x} J_{3-i,z} E^2 \right. \right. \\
& + \left. \left. \left(23E^4 - 12E^2 + 4 \right) J_{i,z} J_{3-i,x} \right) \right) + e_{i,y} \left(12e_{i,x} \left(-16J_{i,z} J_{3-i,x}^2 E^6 - 8J_{i,z} J_{3-i,y}^2 E^6 - 48e_{3-i,z}^2 J_{i,z} E^6 + 8J_{i,z} E^6 - 16J_{i,x} J_{3-i,x} J_{3-i,z} E^6 \right. \right. \\
& - 13J_{i,z} J_{3-i,x}^2 E^4 - 14J_{i,z} J_{3-i,y}^2 E^4 - 54e_{3-i,z}^2 J_{i,z} E^4 + 9J_{i,z} E^4 - 31J_{i,x} J_{3-i,x} J_{3-i,z} E^4 + 13J_{i,y} J_{3-i,y} J_{3-i,z} E^4 - 3J_{i,z} J_{3-i,x}^2 E^2 \\
& + 9J_{i,z} J_{3-i,y}^2 E^2 + 5e_{3-i,x} e_{3-i,z} \left(16E^4 + 31E^2 - 2 \right) J_{i,x} E^2 - 5e_{3-i,y} e_{3-i,z} \left(13E^2 + 2 \right) J_{i,y} E^2 + 12e_{3-i,z}^2 J_{i,z} E^2 - 2J_{i,z} E^2 \\
& + 2J_{i,x} J_{3-i,x} J_{3-i,z} E^2 + 2J_{i,y} J_{3-i,y} J_{3-i,z} E^2 + 2J_{i,z} J_{3-i,x}^2 - 2J_{i,z} J_{3-i,y}^2 + e_{3-i,y}^2 \left(-8E^6 + 16E^4 - 33E^2 + 10 \right) J_{i,z} \\
& + e_{3-i,x}^2 \left(32E^6 + 11E^4 + 27E^2 - 10 \right) J_{i,z} \left) + e_{i,z} \left(-128J_{i,x} J_{3-i,x}^2 E^6 - 32J_{i,x} J_{3-i,y}^2 E^6 + 64J_{i,x} J_{3-i,z}^2 E^6 - 512e_{3-i,z}^2 J_{i,x} E^6 + 32J_{i,x} E^6 \right. \\
& + 192J_{i,z} J_{3-i,x} J_{3-i,z} E^6 - 421J_{i,x} J_{3-i,x}^2 E^4 - 253J_{i,x} J_{3-i,y}^2 E^4 + 176J_{i,x} J_{3-i,z}^2 E^4 - 1876e_{3-i,z}^2 J_{i,x} E^4 + 166J_{i,x} E^4 \\
& + 138J_{i,y} J_{3-i,x} J_{3-i,y} E^4 + 372J_{i,z} J_{3-i,x} J_{3-i,z} E^4 + 36J_{i,x} J_{3-i,x}^2 E^2 - 72J_{i,x} J_{3-i,y}^2 E^2 - 72e_{3-i,z}^2 J_{i,x} E^2 + 12J_{i,x} E^2 - 72J_{i,y} J_{3-i,x} J_{3-i,y} E^2 \\
& - 24J_{i,z} J_{3-i,x} J_{3-i,z} E^2 - 12J_{i,x} J_{3-i,x}^2 + 12J_{i,x} J_{3-i,y}^2 + e_{3-i,y}^2 \left(-32E^6 + 269E^4 + 288E^2 - 60 \right) J_{i,x} \\
& + e_{3-i,x}^2 \left(448E^6 + 1109E^4 - 252E^2 + 60 \right) J_{i,x} - 30e_{3-i,x} \left(2e_{3-i,z} \left(16E^4 + 31E^2 - 2 \right) J_{i,z} E^2 + e_{3-i,y} \left(23E^4 - 12E^2 + 4 \right) J_{i,y} \right) \\
& \left. + 24J_{i,y} J_{3-i,x} J_{3-i,y} \right) \Big] \Big\}. \tag{18d}
\end{aligned}$$

Here, for simplicity, we neglected corrections due to changes of the orbits during the encounter, i.e., we restricted to terms of order $\epsilon_{SA,i}$ and neglected terms of order $\epsilon_{SA,i}^2$ and higher (see [Hamers & Samsing 2019a](#)). However, when comparing to numerical integrations in Section 3.2, we do include the quadrupole-order term $\propto \epsilon_{SA,i}^2$, where the corresponding expression was derived in [Hamers & Samsing \(2019a\)](#).

3 NUMERICAL INTEGRATIONS

In this section, we carry out several numerical integrations to illustrate orbital changes in the two binaries for various parameters, and compare to the analytic expressions of Section 2.4. In Section 3.1, we focus on the backreaction of the outer orbit; in Section 3.2, we consider series of integrations with varying properties of binary 2. An overview of the initial conditions adopted in these sections is given in Table 1. We choose to restrict to systems with equal masses in binary 1, which is motivated by the fact that this eliminates the octuple-order terms (see equation 11b), which would otherwise dominate the hexadecupole-order terms and thus decrease the importance of the hexadecupole-order cross term even further.

Our numerical integrations are based on four-body calculations, as well as calculations based on the equations of motion averaged over the inner orbits (see Section 2.3). The four-body integrations were carried out using the IAS15 integrator within the REBOUND package ([Rein & Liu 2012; Rein & Spiegel 2015](#)). We integrated the inner-averaged equations of motion using ODEINT from the PYTHON SCIPY library, with the relative and absolute tolerances set to 10^{-13} . In both cases of the four-body and inner-averaged integrations, the integration time was set to t_{end} with periaapsis passage (ignoring backreaction) occurring at $t_{\text{end}}/2$, where

$$t_{\text{end}} = \frac{1}{n_3} \left[-4 \operatorname{arctanh} \left(\frac{(E-1) \tan(\beta/2)}{\sqrt{E^2-1}} \right) + \frac{2E\sqrt{E^2-1} \sin \beta}{1+E \cos \beta} \right]. \tag{19}$$

Here, $\beta = f_\theta \arccos(-1/E)$ indicates the fraction of the outer orbit true anomaly θ in the integrations compared to integrating from $t \rightarrow -\infty$ to $t \rightarrow \infty$. Specifically, f_θ corresponds to integrating over true anomaly θ from $-f_\theta \arccos(-1/E)$ to $f_\theta \arccos(-1/E)$, with $f_\theta = 1$ corresponding to integrating from $t \rightarrow -\infty$ to $t \rightarrow \infty$. We have checked our results for convergence with respect to f_θ .

	m_1	m_2	m_3	m_4	a_1	a_2	Q	e_1	e_2	e_3	i_1	i_2	ω_1	ω_2	Ω_1	Ω_2	θ_1	θ_2	f_θ	
Fig. 2	10	10	5	5	1.0	1.5	20	0.9	0.5	1.5	90	0.01	45	0.01	0.01	0.01	0.01	0.01	0.01	0.98
Fig. 3	10	10	5	5	1.0	0.5-3	20	0.1	0.4	1.5	90	0.01	45	0.01	0.01	0.01	0.01	0.01	0.01	0.98
Fig. 4	10	10	5	5	1.0	0.5-3	20	0.1	0.4	1.5	90	0.01	45	0.01	0.01	0.01	0.01	0.01	0.01	0.98
Fig. 5	10	10	5	5	1.0	0.5-3	20	0.9	0.4	1.5	90	0.01	45	0.01	0.01	0.01	0.01	0.01	0.01	0.98
Fig. 6	10	10	5	5	1.0	0.5-3	20	0.9	0.4	1.5	90	57	45	120	0.01	0.01	0.01	0.01	0.01	0.98
Fig. 7	10	10	5-9.1	0.91-5	1.0	2	20	0.1	0.4	1.5	90	0.01	45	0.01	0.01	0.01	0.01	0.01	0.01	0.98
Fig. 8	10	10	5	5	1.0	2	20	0.1	0.4	1.5	90	0.01-70	45	0.01	0.01	0.01	0.01	0.01	0.01	0.98

Table 1. Values of parameters used in the numerical integrations. Inclinations, arguments of periapsis, and longitudes of the ascending node are indicated with i_i , ω_i and Ω_i , respectively (our reference frame is the x, y -plane, and the reference direction is the x -direction). The angles θ_1 and θ_2 are the true anomalies of orbits 1 and 2 (used only in the four-body integrations); f_θ indicates the fraction of the outer orbit true anomaly θ in the integrations compared to integrating from $t \rightarrow -\infty$ to $t \rightarrow \infty$ (see equation 19). Units of all angles ($i_1, i_2, \omega_1, \omega_2, \Omega_1, \Omega_2, \theta_1$ and θ_2) are degrees. Units of masses are M_\odot and distances are measured in AU (note, however, that our system is scale free).

Several PYTHON scripts to carry out the four-body and inner-averaged integrations and to compute the analytic expressions are freely available¹.

3.1 Changes of the outer orbit

As discussed in Sections 2.2.1 and 2.4.1, both binaries can affect the outer orbit and cause the latter to deviate from purely Keplerian motion. Consequently, this can affect the eccentricity and angular-momentum changes of the inner orbits, which we refer to as ‘backreaction’. In Fig. 2, we show the time evolution of the orbital elements (semimajor axes, eccentricities and inclinations) of the three orbits. The top (bottom) nine panels correspond to the situation in which the backreaction terms to quadrupole order (see the expression for $\ddot{\mathbf{r}}_3$ in equation 9) were included (excluded).

In each set of nine panels, the top row shows the semimajor axes. The four-body integrations (solid green lines) show tiny fluctuations in the semimajor axes near periapsis (note that in the top-left panel, +1 should be added in the y -axes). The inner-averaged integrations (black dashed lines) show no change in a_1 and a_2 , as an immediate consequence of orbit averaging. When backreaction is included, the inner-averaged integrations give a fluctuation in a_3 near periapsis with no net change, and which agrees with the four-body integrations. The fact that the semimajor axes are conserved is expected for this system, which is well within the secular regime.

The middle and bottom rows in each set of nine panels show the eccentricities and inclinations, respectively. Without backreaction, e_3 and i_3 in the inner-averaged integrations remain constant by construction, whereas the four-body integrations show that there is a net change in these quantities—the net change in e_3 is tiny, whereas it is more significant (but still very small) in i_3 , with $\Delta i_3 \approx 0.06^\circ$ in this case. With backreaction included, the inner-averaged integrations agree with the four-body integrations in terms of e_3 and i_3 . Also, the analytic prediction for Δi_3 agrees with the numerical results.

Moreover, in terms of the inner orbit eccentricities and inclinations from the inner-averaged integrations and comparing the top and bottom set of nine panels, it is clear that the backreaction terms have no appreciable effect (the only noticeable effect is a slight different in i_2 of $\approx 0.002^\circ$, as shown in the bottom-middle panel of the low set of nine panels).

3.2 The impact of the ‘binarity’ of the companion

Here, we carry out several series of integrations to investigate the effect that the ‘binarity’ of orbit 2 has on the eccentricity change of orbit 1. All initial conditions can be found in Table 1.

In Fig. 3, we vary a_2 , keeping all other parameters fixed. Evidently, as $a_2 \rightarrow 0$, we recover the limit of an encounter of a binary with a single point mass. First of all, note that the eccentricity changes in orbit 1 are very weakly dependent on a_2 : varying a_2 between 0.5 and 3 AU affects Δe_1 by only $\sim 10^{-5}$. Even for the largest value of a_2 considered, it is still a good approximation to consider orbit 2 as a point mass in the computation of Δe_1 (see the red horizontal dot-dashed line in Fig. 3, which shows the corresponding analytic value assuming binary 2 is a point mass). Note that if a_2 is much larger than 3 AU, the system would no longer be in the secular regime (cf. equation 6). The eccentricity of orbit 2 changes much more appreciably and according to a power law, which is expected given that a_2 is varied in this series of integrations (e.g., Heggie & Rasio 1996).

The inner-averaged integrations generally agree with the four-body results, i.e., Δe_1 increases with increasing a_2 with our choice of initial conditions. Some deviations are apparent at specific values of a_2 , as well as for larger values of a_2 . The latter can be explained by the fact that $\epsilon_{SA,2}$ is approaching unity as a_2 increases, with $\epsilon_{SA,2} \approx 0.017$ if $a_2 = 3$ AU, i.e., the system gradually becomes less secular. The discrepancies at smaller values of a_2 are likely due to mean-motion resonances (MMRs) between the two inner orbits. This is suggested by their occurring locations in a_2 , which correspond to various MMRs and which are indicated with vertical black dashed lines. Specifically, we show the $1 : \alpha$ resonances between orbits 1 and 2, where $\alpha \in \{1, 2, 3, 4\}$; setting $P_1 = \alpha P_2$, where P_i denotes orbital period and α is a dimensionless factor, implies

$$a_2 = a_1 \left[\alpha^2 (M_2/M_1) \right]^{1/3}. \quad (20)$$

¹ https://github.com/hamers/flybys_bin

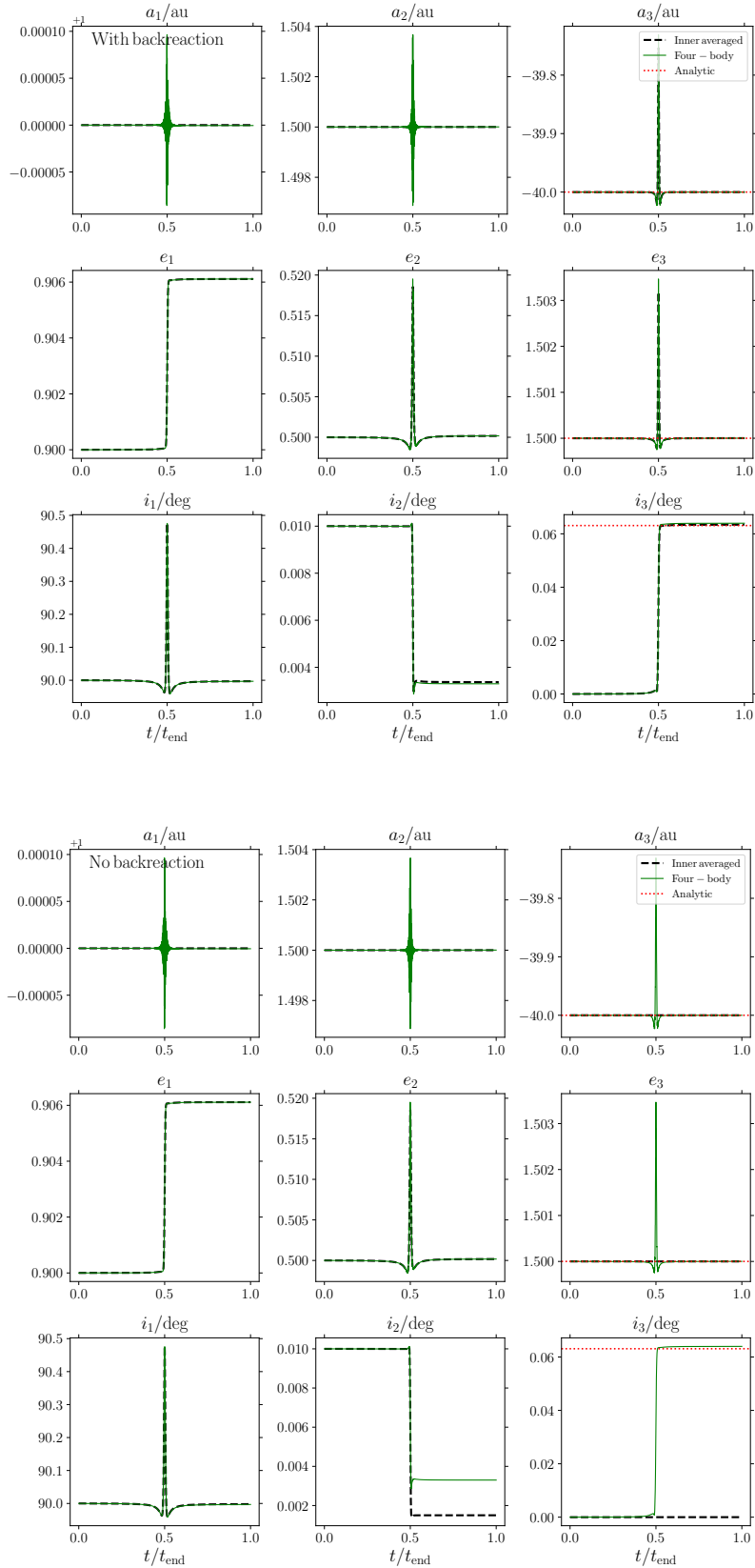


Figure 2. Evolution of the orbital elements of the three orbits as a function of time (normalised to the integration time, t_{end} , see equation 19). See Table 1 for the initial conditions. The backreaction terms were included in the top nine panels, and excluded in the bottom nine panels. In each set of nine panels, the top row shows the semimajor axes, the middle row shows the eccentricities, and the bottom row shows the inclinations. Note that, initially, $i_3 = 0$ by the choice of the coordinate system. Solid green lines correspond to four-body integrations and black dashed lines to integrations averaged over the inner orbit (but not the outer orbit). In the third column, red dotted lines show analytic results for the net changes in the outer orbit (see Section 2.4.1).

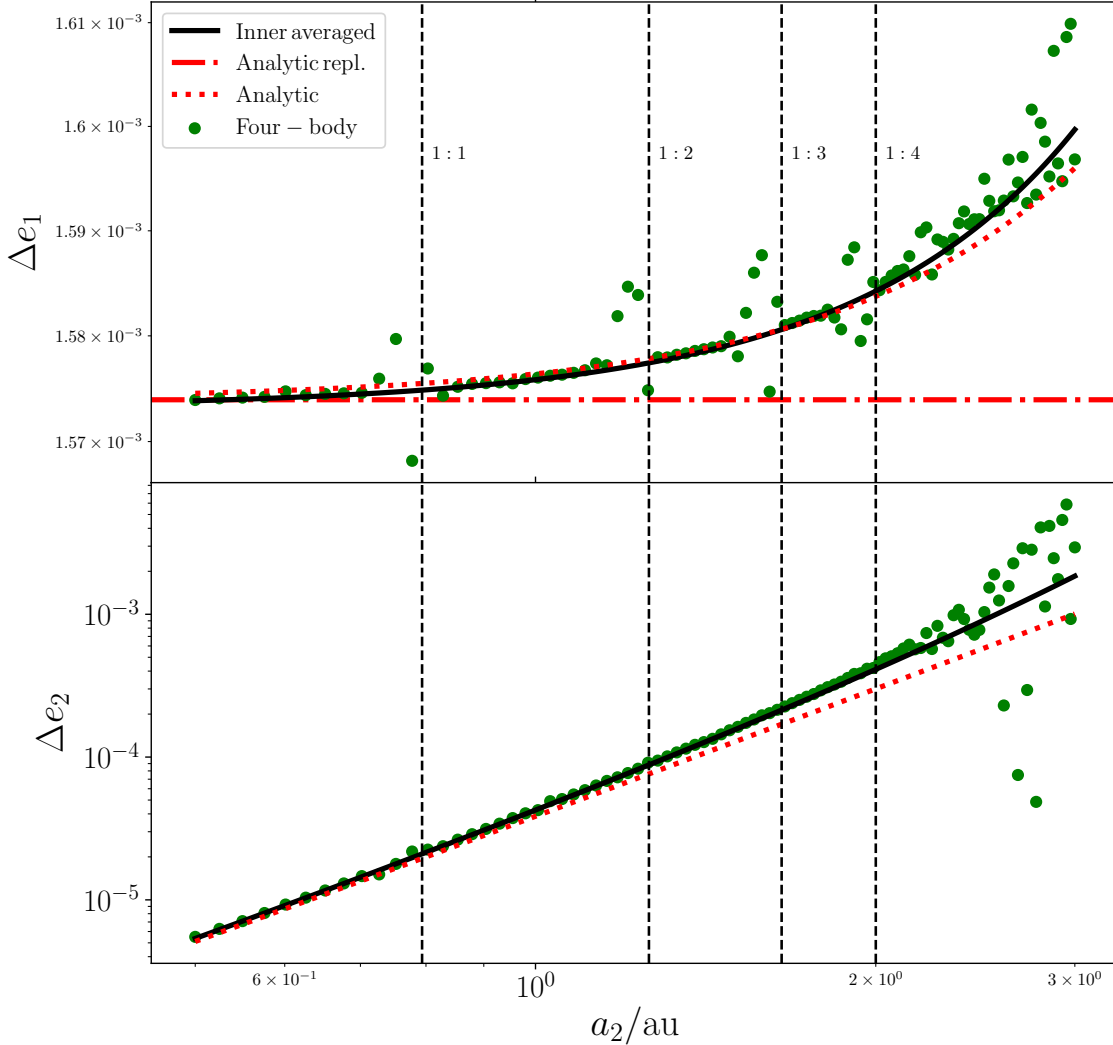


Figure 3. Scalar eccentricity changes in orbits 1 (top panel) and 2 (bottom panel) as a function of a_2 . See Table 1 for the initial conditions. Green dots correspond to four-body integrations, solid black lines to inner-averaged integrations (‘Inner averaged’ in the legend), and red lines to analytic expressions (see Section 2.4.2). For the red dotted lines (‘Analytic’ in the legend), the hexadecupole-order cross term is included, whereas it is not for the horizontal red dot-dashed line (‘Analytic repl.’, i.e., ‘Analytic replaced’ in the legend). In other words, orbit 2 is considered to be a point mass in the ‘Analytic repl.’ horizontal red dot-dashed lines.

The red dotted lines in Fig. 3 show the analytic results from Section 2.4.2 with the inclusion of terms up to and including hexadecupole order (and including the cross term), as well as the quadrupole-order term that is second order in $\epsilon_{SA,i}$ (see Hamers & Samsing 2019a). Overall, these analytic expressions agree with the numerical results, although some deviation can be seen, especially for larger a_2 . This can be attributed to the fact that the analytic expressions do not fully take into account the changing e_i during the encounter (only to second order in $\epsilon_{SA,i}$, and at quadrupole expansion order). Although it is possible in principle to derive more accurate expressions, they are excessively long and so are not practical (see, e.g., table 1 of Hamers & Samsing 2019b).

In Fig. 4, we consider the same series as in Fig. 3, but include only inner-averaged numerical integrations, and compare the cases including backreaction on the outer orbit (black solid lines), and without (black dashed lines). As shown, there are only very small differences between the two cases, again illustrating that the backreaction of the inner two orbits on the outer orbit can be neglected.

We show a similar figure to Fig. 3 in Fig. 5, but now with a higher initial value of e_1 . The eccentricity changes are now slightly larger, and the relative importance of MMRs appears to be lower. In Fig. 6, we choose different values of ω_2 and i_2 . With this different choice of relative orbital orientations, the changes in Δe_1 with increasing a_2 are even smaller, on the order of $\sim 10^{-6}$. The different relative orientation between the orbits in this example leads to a decrease in Δe_1 with increasing a_2 , instead of increasing in Figs 3 and 5. Also, MMRs appear to have a larger impact on Δe_1 .

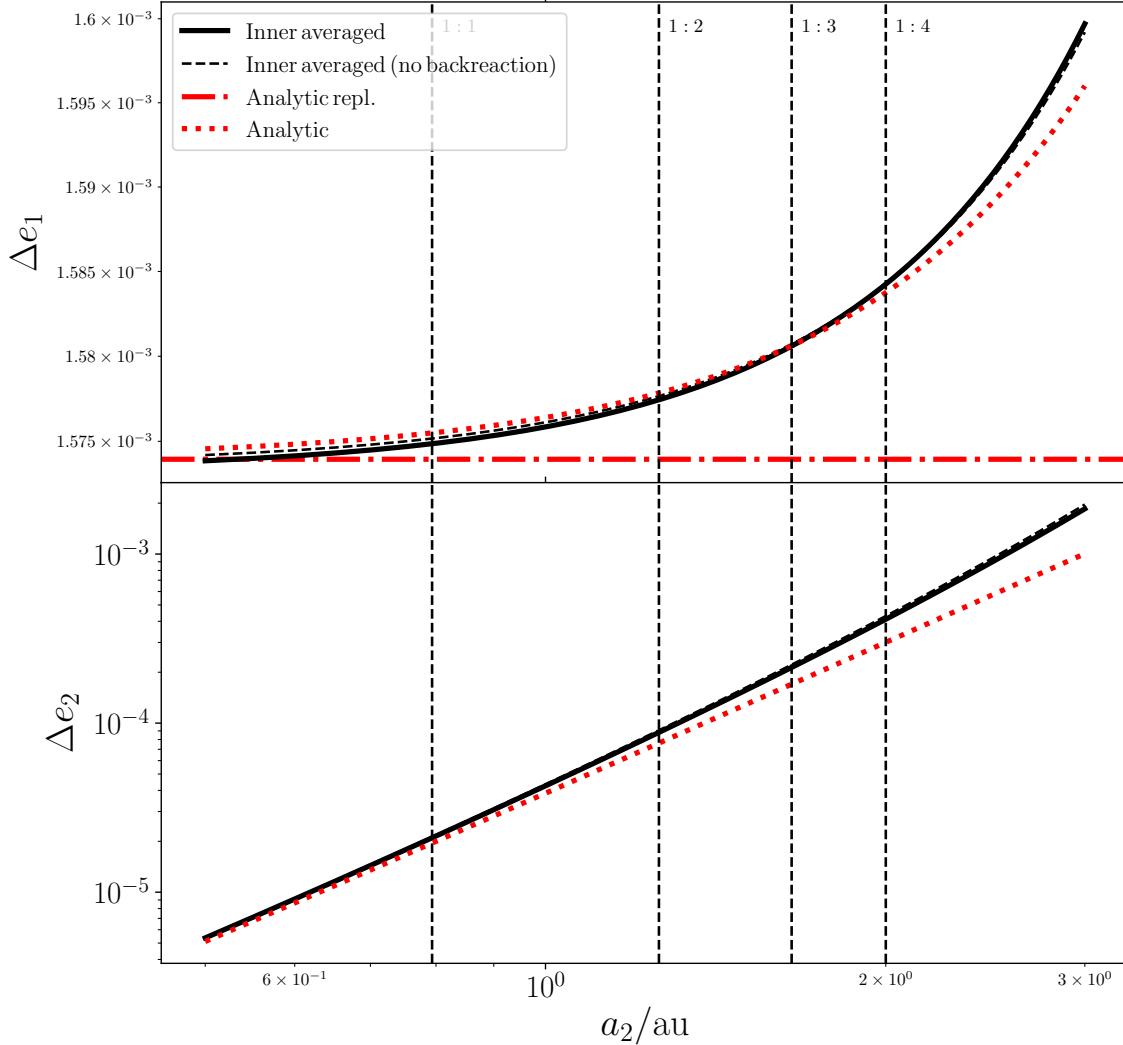


Figure 4. Similar to Fig. 3, but here comparing two cases of inner-averaged numerical integrations: with backreaction on the outer orbit (black solid lines), and without (black dashed lines). The analytic curves (red lines) are the same as in Fig. 3.

In Fig. 7, we fix a_2 but vary $q_2 \equiv m_4/m_3$ instead, keeping the total mass of binary 2, $M_2 = m_3 + m_4$, fixed to $M_2 = 10 M_\odot$. The point-mass limit is approached as $q_2 \rightarrow 0$, and Δe_1 indeed approaches the point-mass value (red horizontal dot-dashed line) as q_2 decreases. The dependence on q_2 , like a_2 , is very weak, with changes in Δe_1 on the order of 10^{-5} . The analytic results including the hexadecupole-order cross term (red dotted lines) agree with the numerical results (both four-body and inner-averaged), except for Δe_2 . This may be related to the omission of higher-order terms in $\epsilon_{SA,i}$. In addition, the four-body integrations do not agree well with the inner-averaged integrations with respect to Δe_2 , which may be due to a breakdown of the inner-averaging approximation.

Lastly, in Fig. 8, we consider the dependence on relative orientation by varying i_2 and fixing the other parameters. The changes in e_1 are again very small, and Δe_1 decreases with increasing i_2 . The analytic expressions agree reasonably with the numerical results.

4 DISCUSSION

4.1 Importance of the cross term

As shown in the above sections, in the expansion of the Hamiltonian of the system, the hexadecupole order is the lowest expansion order at which a term appears that explicitly depends on all three orbits simultaneously (the inner two bound orbits and the outer unbound orbit). This ‘cross term’ gives rise to the largest changes of the secular changes of one binary due to the ‘binarity’ of the other binary. Given that the cross

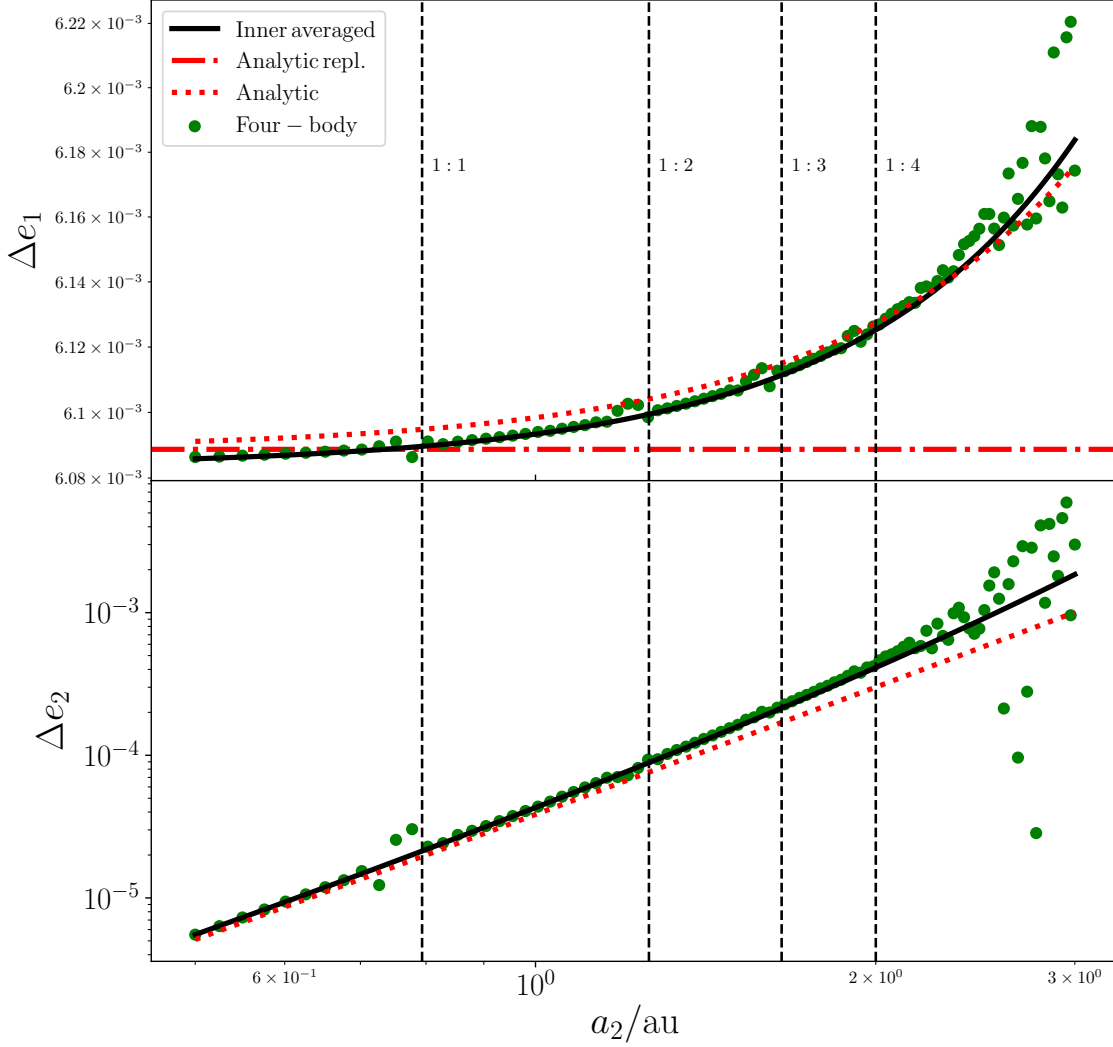


Figure 5. Similar to Fig. 3, but here with higher initial e_1 (see Table 1).

term appears at a high expansion order, the ‘binarity’ effect of the companion binary is typically small and, in most cases, it is well justified to simply apply the known expressions for the secular changes for binary-single interactions (Heggie & Rasio 1996; Spurzem et al. 2009; Hamers 2018; Geller et al. 2019; Hamers & Samsing 2019a,b) with the ‘third body’ mass replaced with the total mass of the companion binary.

Nonetheless, it is informative to explore more generally the importance of the hexadecupole-order cross term in relation to the other terms of interest, i.e., the pairwise quadrupole, octupole, and hexadecupole-order terms. In Fig. 9, we estimate (i.e., within approximately an order of magnitude) the changes in eccentricity and inclination of orbit 1, plotting their rough approximations as a function of Q/a_1 for fixed a_1 , and various values of a_2 . Here, we estimate the eccentricity/inclination changes based on equation (17), ignoring the complex dimensionless functions of e_i , J_i and E and any terms $\mathcal{O}(\epsilon_{SA,i}^2)$. Specifically, we set

$$\Delta e_{1,\text{quad}} \sim \epsilon_{SA,1}; \quad (21a)$$

$$\Delta e_{1,\text{oct}} \sim \epsilon_{SA,1} \epsilon_{\text{oct},1}; \quad (21b)$$

$$\Delta e_{1,\text{hex}} \sim \epsilon_{SA,1} \epsilon_{\text{hex},1}; \quad (21c)$$

$$\Delta e_{1,\text{hex,cross}} \sim \epsilon_{SA,1} \epsilon_{\text{hex,cross},1}, \quad (21d)$$

and similarly for Δi_1 .

Fig. 9 shows that the cross term is small, and can be neglected in most practical situations. It is possible that the cross term exceeds the

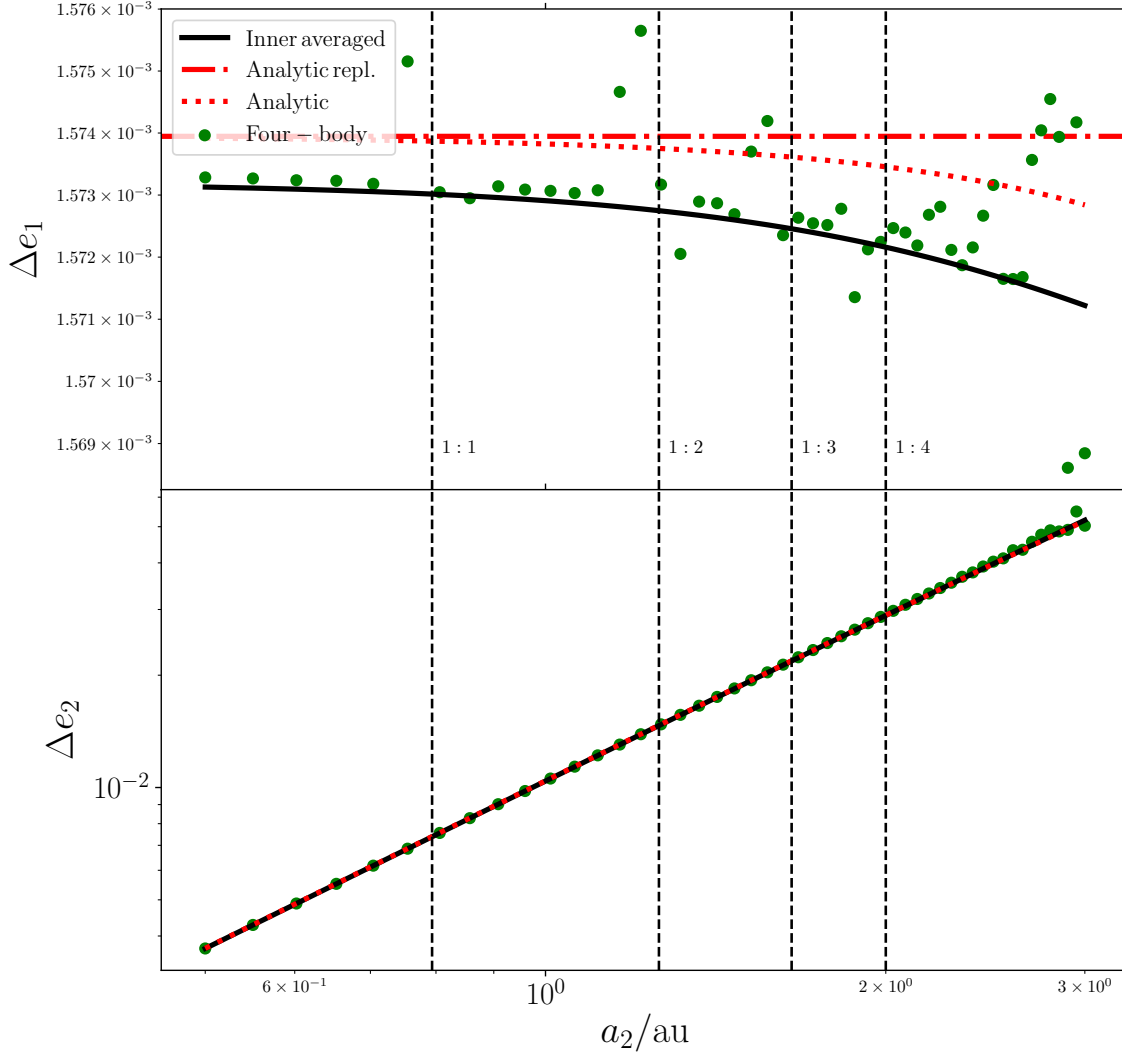


Figure 6. Similar to Fig. 3, but here with different initial ω_2 and i_2 (see Table 1).

contribution from the pairwise hexadecupole-order term, but only in situations with large a_2 ($a_2 = 5$ AU in our examples), in which case the system is barely in the secular limit (note that the smallest Q in Fig. 9 is $Q = 10$ AU, which is only twice as large).

4.2 Limitations of the analytic expressions and the inner-averaged approach

In Section 2.4.2, we derived analytic expressions for the eccentricity changes taking into account the hexadecupole-order cross term, which is the lowest-order term that leads to a direct coupling between the inner two orbits. These expressions agree reasonably with numerical integrations, both four-body integrations and inner-averaged integrations, although the agreement is by no means perfect. Any deviation between the inner-averaged integrations and the analytic expressions arises from the fact that we assumed in Section 2.4.2 that all three orbits are static during the encounter. This approximation can break down, especially when the initial eccentricities are already large (making the inner orbits more susceptible to large secular changes).

Corrections to counter the breakdown of this approximation could be derived to second (and higher) order in $\epsilon_{SA,i}$, as has been done in Hamers & Samsing (2019a). When comparing to numerical results in Section 3, we also included second-order terms in $\epsilon_{SA,i}$, but only to the quadrupole order. Similar expressions to higher orders in $\epsilon_{SA,i}$ give rise to excessively long expressions (see Hamers & Samsing 2019b), which severely reduces their practical usefulness. Moreover, contributions from the second-order terms in $\epsilon_{SA,i}$ at higher expansion orders (octupole, hexadecupole, etc.) become increasingly small. Here, we therefore did not derive new expressions for the eccentricity changes taking into account nonstatic orbits during the encounter for high expansion orders (in particular, for the hexadecupole-order cross term).

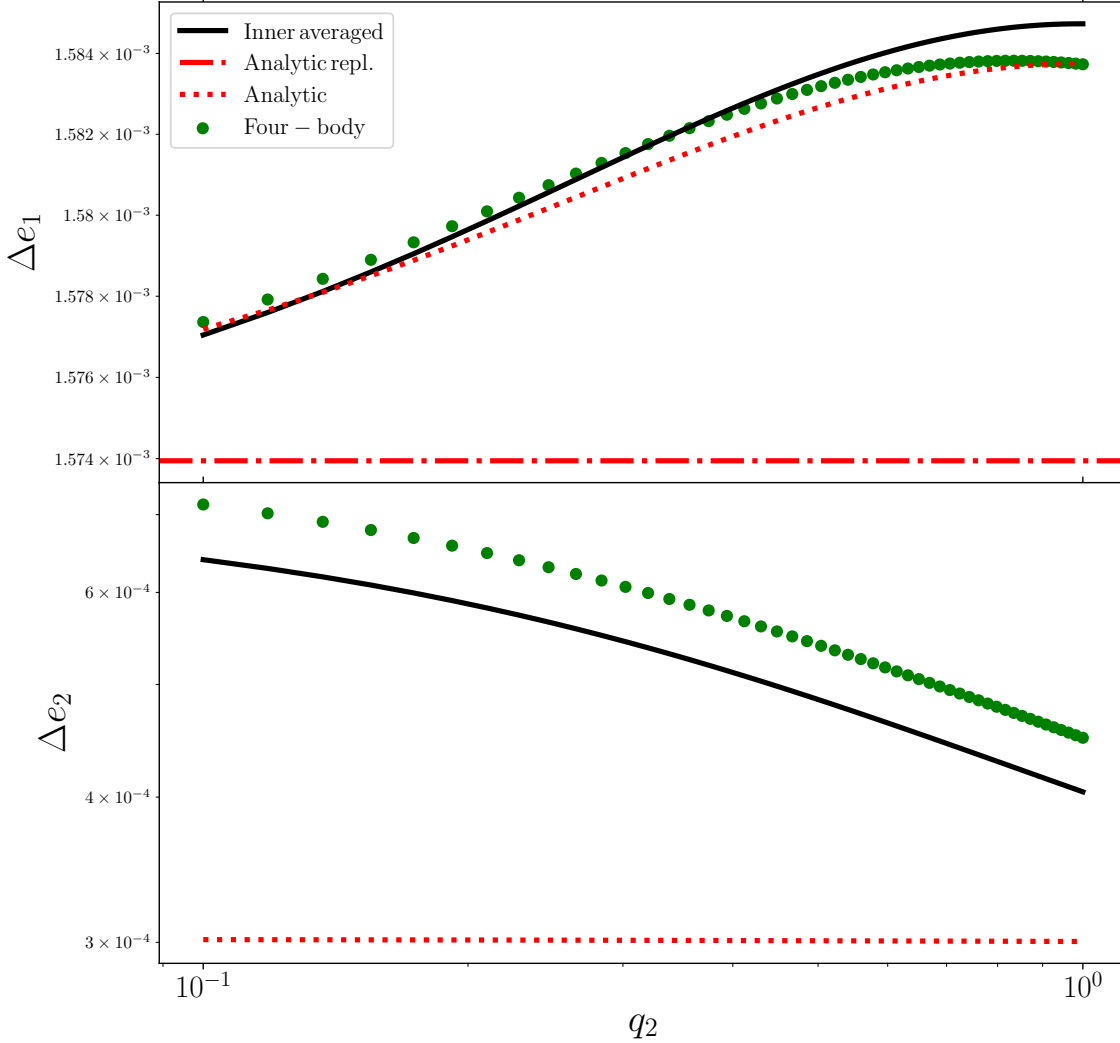


Figure 7. Similar to Fig. 3, but here with fixed a_2 and varying m_3 and m_4 , keeping $M_2 \equiv m_3 + m_4 = 10 M_\odot$ fixed and plotting the eccentricity changes as a function of $q_2 \equiv m_4/m_3$ (see also Table 1).

In addition, we found discrepancies between the four-body integrations and the inner-averaged integrations (on which the fully analytic expressions are based). This is reflected in Fig. 3 and further, where the inner-averaged (black solid lines) and fully-averaged (red dotted lines) show disagreement with the four-body integrations near the mean motion resonance locations, as well as for large a_2 , when the averaging approximation breaks down because a_2 is becoming too large. These discrepancies can be attributed to a breakdown of averaging in the inner orbits. Averaging corrections to the inner orbits as well (see, e.g., Lei 2019) are beyond the scope of this paper.

4.3 Implications for larger- N scattering in the secular limit

We briefly discuss further implications of the main result of this paper, i.e., that, in the secular limit, a binary perturbed by another distant binary is not significantly affected by the quadrupole moment of the companion binary, and that the orbital changes can simply be obtained by applying known results for binary-single encounters and replacing the third body’s mass with the total companion binary mass. With this result in mind, it is clear that an extension to encounters with higher-multiplicity systems in the secular limit can easily be made: for a binary encountering an arbitrary hierarchical system composed of nested orbits one can, to first approximation, apply the secular expressions for binary-single encounters (possibly including higher-order terms in $\epsilon_{SA,1}$) replacing the ‘third body’ mass with the total mass of the encountering hierarchical system. This also implies that any internal evolution of the encountering system does not play any major role, no

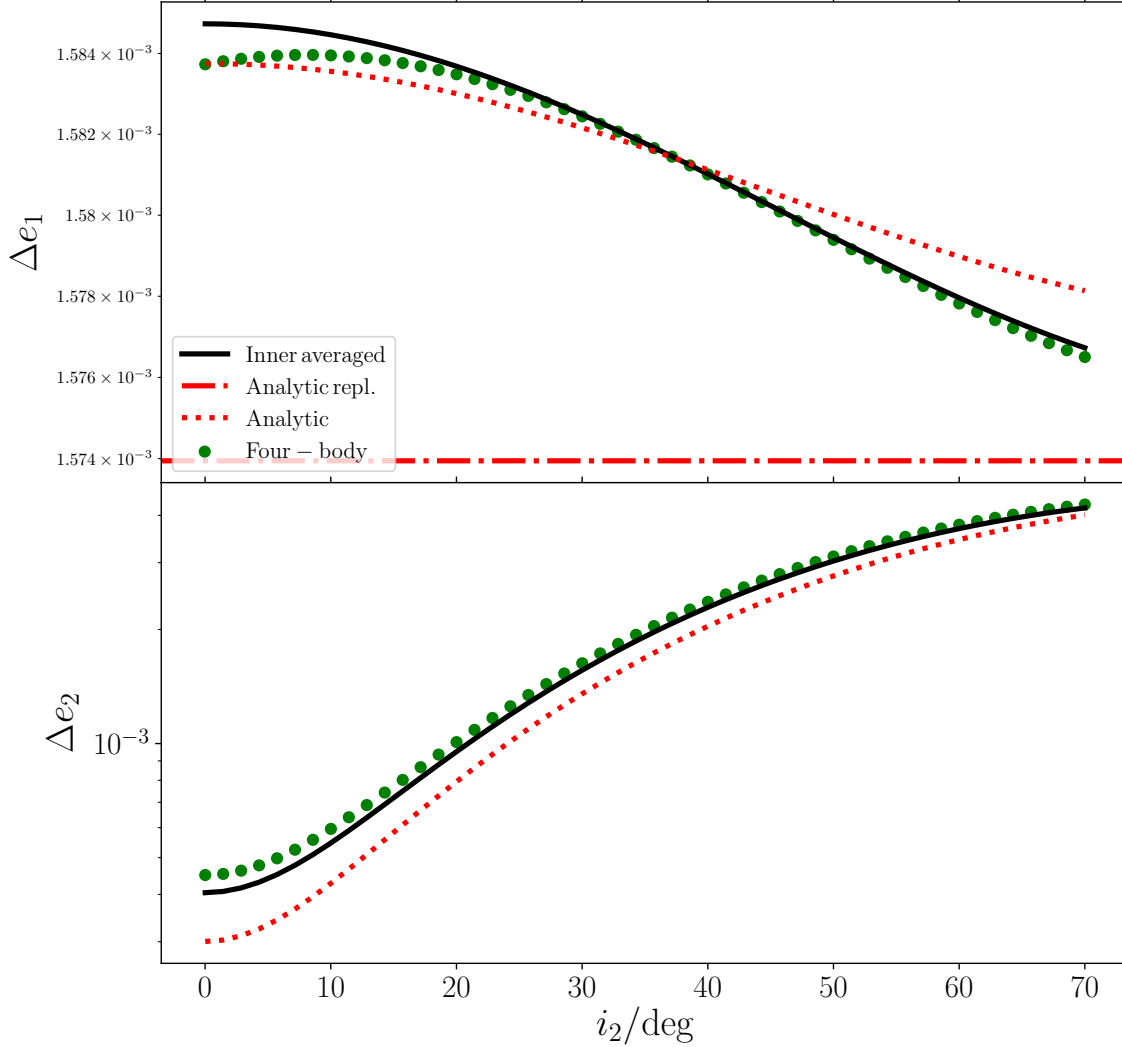


Figure 8. Similar to Fig. 3, but here with fixed a_2 and varying i_2 (see also Table 1).

matter its own evolution timescale in relation to the encounter timescale. For example, a binary encountering a triple results in approximately the same secular effects on the binary compared to the case of a binary encountering a single object with the same mass as the triple.

5 CONCLUSIONS

We studied the dynamical evolution of two binaries approaching each other on unbound orbits. We focused on the ‘secular’ regime, in which the binaries approach each other with a sufficiently large periapsis distance such that the semimajor axes of the two bound orbits do not change appreciably after the encounter, but eccentricity and angular-momentum changes are possible. We carried out numerical integrations, as well as derived analytic results. Our main conclusions are given below.

1. The Hamiltonian, expanded in the small ratios $x_1 = r_1/r_3 \ll 1$ and $x_2 = r_2/r_3 \ll 1$, where r_1 and r_2 are the relative separations of the inner two bound binaries and r_3 is the separation of the ‘outer’ unbound orbit, consists of pairwise terms at the quadrupole and octupole orders ($x_i = 2$ and $x_i = 3$, respectively, for $i \in \{1, 2\}$). Only at the hexadecupole order ($x_i = 4$) there appears a term, the hexadecupole-order cross term, that explicitly depends on the separations of all three orbits. This implies that any effect of the ‘binarity’ of orbit 2 on orbit 1 (i.e., its quadrupole moment) is only exhibited through 1) a backreaction of the outer orbit, r_3 , and 2) high-order expansion terms, starting at the hexadecupole order. We explicitly derived the expanded Hamiltonian (up to and including hexadecupole order) and averaged over the inner two orbits (Section 2.2.2), as well as the corresponding equations of motion (Section 2.3).

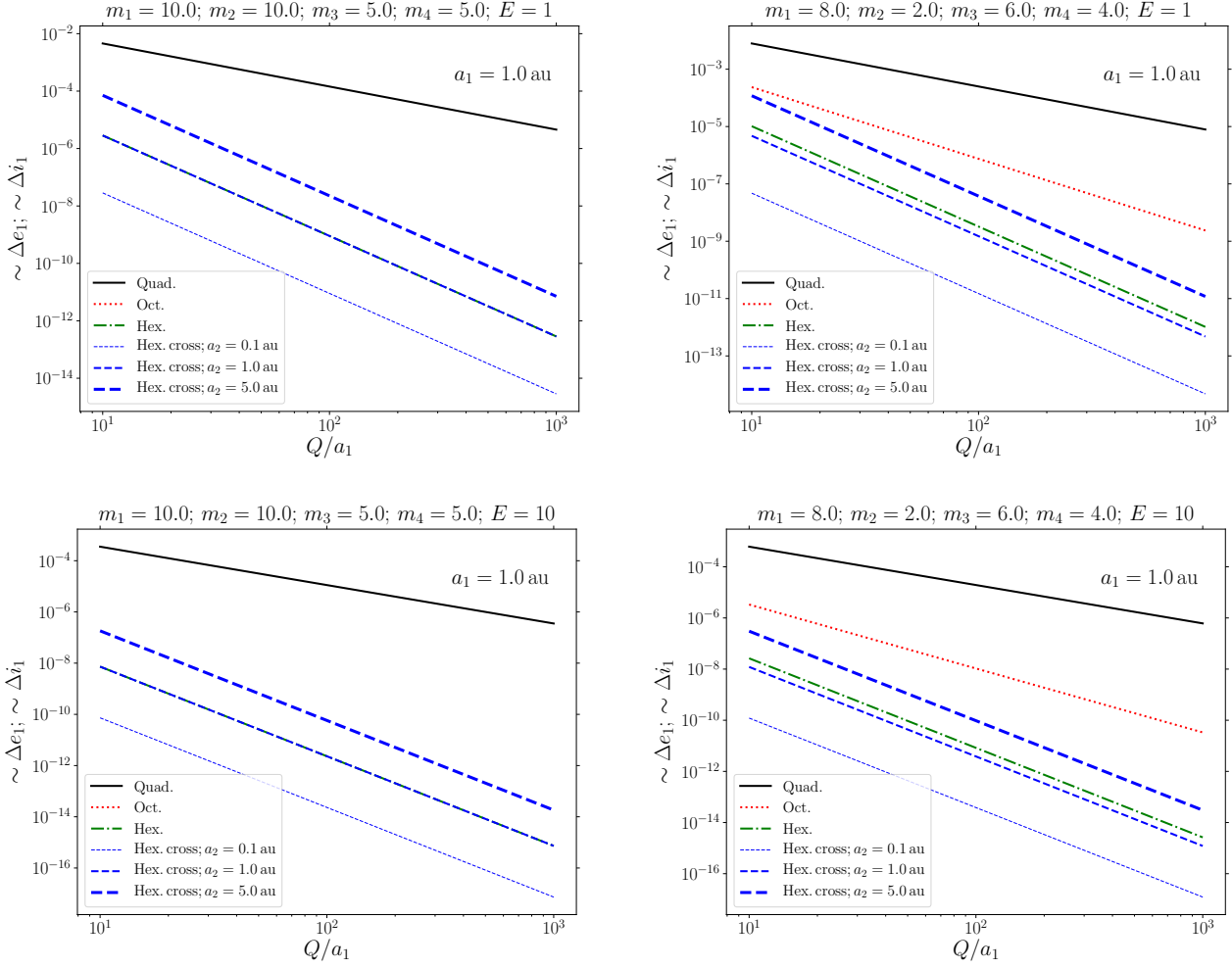


Figure 9. Changes of the eccentricity and inclination of orbit 1 plotted as a function of Q/a_1 for a fixed $a_1 = 1$ AU and different a_2 (the latter being either 0.1, 1.0, or 5.0 AU). We show the contributions from various expansion orders in the Hamiltonian to Δe_1 and Δi_1 , which we roughly estimate (within approximately an order of magnitude) using equation (21a). Each panel corresponds to a certain choice of the masses m_i and the outer orbit eccentricity E , indicated in the top. Note: in the left-hand column, the ‘Oct.’ lines are zero and therefore not shown, since $m_1 = m_2$. Also, the ‘Hex.’ lines coincide exactly with the ‘Hex. cross’ lines at $a_2 = 1$ AU.

2. We derived approximate analytic expressions for the eccentricity and inclination changes of the outer orbit due to the backreaction of orbits 1 and 2 (Section 2.4.1). These expressions show that the backreaction effects are very small, which we confirmed with numerical integrations (Section 3.1).

3. We also derived approximate analytic expressions for the secular effects on the inner orbits taking into account the hexadecupole-order cross term. In particular, the quadrupole moment of the companion orbit gives rise to the secular changes which are on the order of $\epsilon_{SA,1}(a_2/Q)^2[m_3m_4/(m_3+m_4)^2]$, where $\epsilon_{SA,1}$ is the magnitude of the quadrupole-order change (see equation 11a), and a_2 and (m_3, m_4) are the companion binary orbital semimajor axis and component masses, respectively. Here, we largely ignored the fact that the inner orbits change dynamically during the encounter, i.e., we restricted to expressions to first order in the perturbation parameter $\epsilon_{SA,i}$ except for the quadrupole order (see also Hamers & Samsing 2019a). Nevertheless, the analytic expressions generally agree with numerical integrations (Section 3.2).

4. Most importantly, as shown by our analytic and numerical results, the ‘binarity’ of orbit 2, when considering orbit 1, typically leads to only very small eccentricity and inclination changes. To good approximation, one can obtain the secular changes by using the analytic results for binary-single interactions (Heggie & Rasio 1996; Spurzem et al. 2009; Hamers 2018; Geller et al. 2019; Hamers & Samsing 2019a,b) and replacing the mass of the intruding unbound third body with the total mass of binary 2. In other words, the point-mass approximation works well in this case.

Several PYTHON scripts implementing the two numerical integration methods and the analytical results as well as routines used to make all the plots in this paper, are freely available at the link given in Section 3.

ACKNOWLEDGEMENTS

We thank the referee, Douglas Heggie, for a very helpful report. J.S. acknowledges support from the European Unions Horizon 2020 research and innovation programme under the Marie Skłodowska-Curie grant agreement No. 844629. Simulations in this paper made use of the REBOUND code which is freely available at <http://github.com/hannorein/rebound>.

References

- Abbott B. P., et al., 2016a, *Physical Review Letters*, 116, 061102
 Abbott B. P., et al., 2016b, *Physical Review Letters*, 116, 241103
 Abbott B. P., et al., 2017a, *Physical Review Letters*, 118, 221101
 Abbott B. P., et al., 2017b, *Physical Review Letters*, 119, 141101
 Abbott B. P., et al., 2017c, *ApJ*, 848, L12
 Abbott B. P., et al., 2017d, *ApJ*, 851, L35
 Alexander M. E., 1986, *Journal of Computational Physics*, 64, 195
 Antognini J. M. O., Thompson T. A., 2016, *MNRAS*, 456, 4219
 Bacon D., Sigurdsson S., Davies M. B., 1996, *MNRAS*, 281, 830
 Davies M. B., Benz W., Hills J. G., 1993, *ApJ*, 411, 285
 Eggleton P., 2006, *Evolutionary Processes in Binary and Multiple Stars*
 Geller A. M., Leigh N. W. C., Giersz M., Kremer K., Rasio F. A., 2019, *ApJ*, 872, 165
 Goodman J., Hut P., 1993, *ApJ*, 403, 271
 Hamers A. S., 2018, *MNRAS*, 476, 4139
 Hamers A. S., Portegies Zwart S. F., 2016, *MNRAS*, 459, 2827
 Hamers A. S., Samsing J., 2019a, *MNRAS*, 487, 5630
 Hamers A. S., Samsing J., 2019b, *MNRAS*, 488, 5192
 Hamers A. S., Perets H. B., Antonini F., Portegies Zwart S. F., 2015, *MNRAS*, 449, 4221
 Heggie D. C., 1975, *MNRAS*, 173, 729
 Heggie D. C., Hut P., 1993, *ApJS*, 85, 347
 Heggie D. C., Rasio F. A., 1996, *MNRAS*, 282, 1064
 Heggie D. C., Hut P., McMillan S. L. W., 1996, *ApJ*, 467, 359
 Hoffer J. B., 1983, *AJ*, 88, 1420
 Hut P., 1983, *ApJ*, 268, 342
 Hut P., 1993, *ApJ*, 403, 256
 Hut P., Bahcall J. N., 1983, *ApJ*, 268, 319
 Hut P., McMillan S., Romani R. W., 1992, *ApJ*, 389, 527
 Kimpson T. O., Spera M., Mapelli M., Ziosi B. M., 2016, *MNRAS*, 463, 2443
 Kocsis B., Levin J., 2012, *Phys. Rev. D*, 85, 123005
 Lei H., 2019, *MNRAS*, 490, 4756
 Leigh N., Geller A. M., 2012, *MNRAS*, 425, 2369
 Leigh N. W. C., Geller A. M., 2015, *MNRAS*, 450, 1724
 Leigh N., Sills A., 2011, *MNRAS*, 410, 2370
 Leigh N. W. C., Geller A. M., Shara M. M., Garland J., Clees-Baron H., Ahmed A., 2017, *MNRAS*, 471, 1830
 Leigh N. W. C., Geller A. M., Shara M. M., Baugher L., Hierro V., Ferreira D., Teperino E., 2018, *MNRAS*, 480, 3062
 Leonard P. J. T., 1989, *AJ*, 98, 217
 Li G., Adams F. C., 2015, *MNRAS*, 448, 344
 Mapelli M., 2016, *MNRAS*, 459, 3432
 McMillan S., Hut P., 1994, *ApJ*, 427, 793
 McMillan S. L. W., Hut P., 1996, *ApJ*, 467, 348
 Mikkola S., 1983, *MNRAS*, 203, 1107
 Mikkola S., 1984a, *MNRAS*, 207, 115
 Mikkola S., 1984b, *MNRAS*, 208, 75
 O'Leary R. M., Rasio F. A., Fregeau J. M., Ivanova N., O'Shaughnessy R., 2006, *ApJ*, 637, 937
 Portegies Zwart S. F., McMillan S. L. W., 2000, *ApJ*, 528, L17
 Rasio F. A., McMillan S., Hut P., 1995, *ApJ*, 438, L33
 Rein H., Liu S. F., 2012, *A&A*, 537, A128
 Rein H., Spiegel D. S., 2015, *MNRAS*, 446, 1424
 Rodriguez C. L., Morscher M., Pattabiraman B., Chatterjee S., Haster C.-J., Rasio F. A., 2015, *Physical Review Letters*, 115, 051101
 Rodriguez C. L., Chatterjee S., Rasio F. A., 2016, *Phys. Rev. D*, 93, 084029
 Rodriguez C. L., Amaro-Seoane P., Chatterjee S., Rasio F. A., 2018, *Physical Review Letters*, 120, 151101
 Ryu T., Leigh N. W. C., Perna R., 2017, *MNRAS*, 467, 4447
 Samsing J., 2018, *Phys. Rev. D*, 97, 103014
 Samsing J., Ramirez-Ruiz E., 2017, *ApJ*, 840, L14
 Samsing J., D'Orazio D. J., Askar A., Giersz M., 2018a, arXiv e-prints, p. arXiv:1802.08654
 Samsing J., MacLeod M., Ramirez-Ruiz E., 2018b, *ApJ*, 853, 140
 Samsing J., Askar A., Giersz M., 2018c, *ApJ*, 855, 124
 Samsing J., Hamers A. S., Tyles J. G., 2019, *Phys. Rev. D*, 100, 043010
 Sigurdsson S., Hernquist L., 1993, *Nature*, 364, 423

- Sigurdsson S., Phinney E. S., 1993, *ApJ*, **415**, 631
Spurzem R., Giersz M., Heggie D. C., Lin D. N. C., 2009, *ApJ*, **697**, 458
Zevin M., Samsing J., Rodriguez C., Haster C.-J., Ramirez-Ruiz E., 2019, *ApJ*, **871**, 91
Ziosi B. M., Mapelli M., Branchesi M., Tormen G., 2014, *MNRAS*, **441**, 3703